J. Fluid Mech. (2010), *vol.* 649, *pp.* 233–273.
doi:10.1017/S0022112009993430

Large-scale structures in turbulent and reverse-transitional sink flow boundary layers

SHIVSAI AJIT DIXIT† AND O. N. RAMESH‡

Department of Aerospace Engineering, Indian Institute of Science, Bangalore 560012, India

(Received 16 March 2009; revised 11 November 2009; accepted 11 November 2009)

Aspects of large-scale organized structures in sink flow turbulent and reverse-transitional boundary layers are studied experimentally using hot-wire anemometry. Each of the present sink flow boundary layers is in a state of 'perfect equilibrium' or 'exact self-preservation' in the sense of Townsend (*The Structure of Turbulent Shear Flow*, 1st and 2nd edns, 1956, 1976, Cambridge University Press) and Rotta (*Progr. Aeronaut. Sci.*, vol. 2, 1962, pp. 1–220) and conforms to the notion of 'pure wall-flow' (Coles, *J. Aerosp. Sci.*, vol. 24, 1957, pp. 495–506), at least for the turbulent cases. It is found that the characteristic inclination angle of the structure undergoes a systematic decrease with the increase in strength of the streamwise favourable pressure gradient. Detectable wall-normal extent of the structure is found to be typically half of the boundary layer thickness. Streamwise extent of the structure shows marked increase as the favourable pressure gradient is made progressively severe. Proposals for the typical eddy forms in sink flow turbulent and reverse-transitional flows are presented, and the possibility of structural self-organization (i.e. individual hairpin vortices forming streamwise coherent hairpin packets) in these flows is also discussed. It is further indicated that these structural ideas may be used to explain, from a structural viewpoint, the phenomenon of *soft* relaminarization or reverse transition of turbulent boundary layers when subjected to strong streamwise favourable pressure gradients. Taylor's 'frozen turbulence' hypothesis is experimentally shown to be valid for flows in the present study even though large streamwise accelerations are involved, the flow being even reverse transitional in some cases. Possible conditions, which are required to be satisfied for the safe use of Taylor's hypothesis in pressure-gradient-driven flows, are also outlined. Measured convection velocities are found to be fairly close to the local mean velocities (typically 90 % or more) suggesting that the structure gets convected downstream almost along with the mean flow.

1. Introduction

For turbulent shear flows, the role of large-scale organized motions assumes great importance, as they are responsible for major transport of mass, momentum, energy and species across large extents of the flow (for a comprehensive review of coherent structures, see Hussain 1983; Robinson 1991). While the literature is replete with the study of organized structures or eddy structures in zero-pressure-gradient (ZPG)

† Present address: Department of Mechanical Engineering, MKSSS's Cummins College of Engineering for Women, Karvenagar, Pune, Maharashtra 411052, India.
‡ Email address for correspondence: onr@aero.iisc.ernet.in

turbulent boundary layers, the effect of the streamwise pressure gradient on the eddy structure – especially the favourable pressure gradient (FPG) – is not so commonly studied. The present work focuses on large-scale structures in turbulent and reverse-transitional sink flow boundary layers. Towards this we begin with a brief survey of the literature on organized structures in turbulent boundary layers, and since the literature is vast (dealing with different aspects of organized motions), only the relevant references will be discussed.

Townsend (1976) has postulated the existence of the so-called attached eddies in the case of turbulent boundary layers that represent the large-scale organized motion. Smoke-flow visualization studies by Head & Bandyopadhyay (1981) have revealed that a ZPG turbulent boundary layer indeed possesses a large population of identifiable hairpin-type vortices that closely resemble the attached eddies of Townsend (1976). From the photographs, they have reported an average eddy inclination of about 45° from the wall which mainly corresponds to the outer region of the flow.

Following this, Perry & Chong (1982) have shown that many aspects of near-wall turbulent statistics such as intensities and spectra may be calculated by postulating a population of hairpin or horseshoe or Λ vortices (inclined at 45° to the wall). Subtle differences between these eddy types are discussed by Robinson (1991). Perry, Henbest & Chong (1986) have further extended the approach of Perry & Chong (1982) to include the outer region of the turbulent boundary layer as well. This attached-eddy approach has been used further by Perry, Marusic & Li (1994) for addressing the closure problem and by Perry, Marusic & Jones (2002) for predicting the streamwise evolution of turbulent boundary layers in arbitrary pressure gradients.

Brown & Thomas (1977) have investigated the inclination angle of the large-scale structure in a ZPG turbulent boundary layer using hot-wire (HW) anemometry. They have used an array of four HW sensors, separated in the wall-normal direction, in conjunction with a hot-film sensor (for wall-shear stress signature) placed on the wall. The temporal cross-correlation coefficient between the wall-shear stress fluctuation and the streamwise velocity fluctuation has been measured by acquiring signals from all the five sensors simultaneously. For each particular wall-normal distance, the streamwise location corresponding to peak value of the temporal cross-correlation coefficient has been obtained by trial and error. From these measurements, they have shown that the average inclination of the large-scale structure is about 18° and that the convection velocity of the structure is about 0.8 times the free-stream velocity. Similar results for the structure inclination have been reported by Wark & Nagib (1991).

Adrian, Meinhart & Tomkins (2000) have presented extensive particle image velocimetry (PIV) measurements and analysis of the vortex structure of a ZPG turbulent boundary layer. They have shown that hairpin vortices in a ZPG turbulent boundary layer self-organize to form what are called spatially coherent vortex packets, and these packets of varying sizes and 'ages' populate the entire boundary layer. They have noted that the inclinations of individual hairpins in these packets are small close to the wall (typically 15° or so) and increase to large angles (typically 45° or even more if the packet is in the outer layer) away from the wall. The 'heads' of hairpins in a given packet, close to the wall, appear to be located on a ramp-like line which has a shallow inclination of about 12° with respect to the wall; this inclination may be referred to as the packet inclination. The length and the wall-normal extent of these packets are observed to depend on their 'age'. It is also observed that the growth of smaller and younger packets in the environment of larger and older packets (which were generated upstream) is a prominent feature of the logarithmic region of

the mean velocity profile for a ZPG turbulent boundary layer flow. The number of hairpins in a packet is often of the order of 10. It is also remarked in this paper that the two-point correlation studies such as those of Brown & Thomas (1977) mostly relate the measured structure inclinations to the 'backs' of outer layer bulges (see figure 4 from Brown & Thomas 1977) and not generally to the packet inclination mentioned above. It is further noted that the outer layer bulges are essentially related to the hairpin packets especially at low Reynolds numbers, suggesting that for low-Reynolds-number ZPG turbulent boundary layer flows, it may not be inappropriate to relate the measured structure inclinations to the packet inclinations.

Following this work, Christensen & Adrian (2001) have shown that the instantaneous picture of self-organization of hairpins into packets is valid even in the mean sense. They have used linear stochastic estimation for estimating conditionally averaged two-dimensional velocity field from the instantaneous snapshots of a turbulent channel flow at two different Reynolds numbers. Also they have noted that the structural features of turbulent pipe flow, channel flow and boundary layers (ZPG) are very similar below $y/\delta = 0.6$, i.e. mainly in the inner and overlap regions. Their results show that even in the average sense there exists dominant self-organization of hairpins into vortex packets that typically have shallow inclinations of about 12°–13° with the wall. This work therefore connects the instantaneous and mean viewpoints and is thus important in that respect.

Marusic (2001) has shown that the attached-eddy calculations of a ZPG turbulent boundary layer are in better agreement with the experiments if one uses packets of slanted Π-eddies instead of ordinary Π-eddies as seen in figure 3 of Marusic (2001). These structures are consistent with those observed by Adrian *et al.* (2000). It is further remarked that results for the outer layer are relatively insensitive to the use of packets or individual hairpins; results in the near-wall region (inclusive of the log layer) however show marked improvement when hairpin packets are used for calculations.

Colella & Keith (2003) have performed experiments on a flat plate in a towing tank with water as the working fluid. They have used an array of shear stress sensors on the wall in conjunction with a single HW probe to measure the cross-correlation between fluctuating wall-shear stress and streamwise velocity fluctuation. Their inferred structure angle corresponds well with that reported by Brown & Thomas (1977).

Ganapathisubramani, Longmire & Marusic (2003) have presented stereo-PIV measurements in streamwise-spanwise planes of a ZPG turbulent boundary layer. They have used a feature extraction algorithm for identifying large-scale structures all across the boundary layer. They have observed that the logarithmic layer contains significant streamwise spatial organization of hairpin vortices into coherent packets extending up to about 2δ in the streamwise direction. This is consistent with the findings of Adrian *et al.* (2000). Interestingly however, they have reported a breakdown of such structural organization beyond the log layer (in the wake region of the outer layer) where individual hairpins exist but no packets (this observation is shown to be consistent with the calculations of Marusic 2001). They have concluded this on the basis of the absence of long low-momentum zones which are considered to be a typical signature of the hairpin packets. They have also quantified the contribution of coherent packets to the Reynolds shear stress which they have observed to be more than 25 % (of the total Reynolds shear stress), indicating that the packets are responsible for a significant portion of turbulent transport. Following this study, Ganapathisubramani *et al.* (2005) have presented extensive two-point

velocity correlation data obtained from stereo-PIV investigations at various heights in a ZPG turbulent boundary layer flow. They have found that the contours of various correlations in streamwise, cross-stream and inclined planes (45° and 135°) may be interpreted in support of the hairpin packet paradigm and are in general consistent with the previous findings of Ganapathisubramani *et al.* (2003).

Recently Marusic & Heuer (2007) have conducted structure inclination angle measurements in the logarithmic region of laboratory ZPG turbulent boundary layers as well as in the near-neutral atmospheric surface layer at the Utah salt flats. Their results show that the inferred structure inclination angle is about 14°–15° and is remarkably invariant over the wide range of Reynolds numbers (almost three decades) investigated.

A highly resolved direct numerical simulation (DNS) of a spatially developing ZPG boundary layer flow going from the Blasius case to fully turbulent flow through an intermediate transition regime has been carried out very recently by Wu & Moin (2009). Their results show remarkable evidence (though instantaneous) for the existence of hairpin vortices populating the entire turbulent boundary layer (see figures 3*e* and 3*f* from their paper). Furthermore it is noted in this paper that the hairpins are mostly symmetric as opposed to the previous notion that symmetric hairpins are rarely formed (see Robinson 1991).

The point to be noted in all the above-mentioned investigations is that the emphasis has mostly been on ZPG turbulent boundary layer flow, perhaps because even for this canonical flow, the structural details have not been fully understood. It appears that there have not been as systematic and extensive studies on pressure-gradient-driven turbulent boundary layer flows that have been reported in the literature as for the ZPG flows. There are only very few HW anemometry studies on the inclination of structures in adverse-pressure-gradient (APG) turbulent boundary layer flows – such as those of Krogstad & Skåre (1995) and Thomas & Brown (G. Brown 2009, private communication). Krogstad & Skåre (1995) have presented two-point velocity correlation measurements in (i) an APG near-equilibrium turbulent boundary layer that is close to separation and (ii) a ZPG turbulent boundary layer. They have noted that the structure inclination is about 45° almost all through the boundary layer in the APG case (see figure 5*a* from Krogstad & Skåre 1995). This is to be contrasted with the corresponding ZPG results in which the structure inclination angle is relatively shallow close to the wall and reaches the typical value of about 45° only in the outer region of the turbulent boundary layer (see figure 5*b* from Krogstad & Skåre 1995). These results correspond to the wake region of the outer layer (figure 1 from Krogstad & Skåre 1995) and therefore are related to what are called type B eddies in the classification of Perry *et al.* (2002). Very recently Lee & Sung (2009) have reported a comparative DNS study of the structure of ZPG and APG turbulent boundary layers with R_θ in the range 1000–1400. Their results show evidence towards structural organization in the form of streamwise coherent hairpin packets similar to what Adrian *et al.* (2000) and Christensen & Adrian (2001) have reported. Further Lee & Sung (2009) have noted that the characteristic inclination of instantaneous as well average (linear-stochastically estimated) vortex packets increases in APG (about 18°) in comparison with that in ZPG (about 13°). They have also made an interesting observation that the average streamwise spacing between the hairpins in a packet, when scaled with the boundary layer thickness, increases in an APG as compared with the ZPG case.

There appears to be hardly any structural investigation concerning FPG flows with the exception of Blackwelder & Kovasznay (1972) to name one of the few. They have

investigated large-scale motion inside a relaminarizing turbulent boundary layer for which the FPG changes continuously in the streamwise direction (non-equilibrium flow). From the measured contours of space–time correlations they have concluded that the large-eddy structure does not change significantly even after passing through the strongest part of the FPG, save for some interesting aspects of the contours involving fluctuating component of the wall-normal velocity. They have not however reported the structure inclination measurements for their FPG flow.

Thus it would be of interest, perhaps as a first step, to systematically characterize the large-scale structure orientation with pressure gradient as a parameter. This would shed light on the behaviour of turbulent boundary layer flows in pressure gradients. Furthermore, such results would be useful as input for modelling the near-wall region of pressure-gradient-driven turbulent boundary layers. Similar results in ZPG situations have been used as input for modelling (see Piomelli *et al.* 1989; Marusic, Kunkel & Porté-Agel 2001).

It is clear that such characterization of the large-scale structure should be carried out, at least initially, in a pressure-gradient-driven turbulent boundary layer flow where the upstream history effects are negligibly small. This would ensure that the response of the structure is simply related to the changes in pressure gradient without the additional complication of history effects. Thus one must focus attention on what are known as equilibrium or self-preserving turbulent boundary layer flows (Rotta 1962; Townsend 1976). The simplest (i.e. perhaps the easiest to establish experimentally) equilibrium turbulent boundary layer flow is the so-called sink flow – where the boundary layer flow experiences streamwise acceleration inside a convergent channel bounded by smooth and plane walls (see figure 1 from Dixit & Ramesh 2008). One may observe that all the mean streamlines of this flow are radial, intersecting each other at the location of the apparent line sink. Further, mean edge of this turbulent boundary layer is also a mean streamline, indicating that the mean entrainment into the turbulent boundary layer is zero. Interestingly, this is the only smooth-walled turbulent boundary layer configuration where the boundary layer is in 'perfect equilibrium' (see Rotta 1962; Townsend 1976); i.e. the mean velocity and the turbulent statistics scale perfectly with inner as well as outer 'local' flow scales as may be seen from the equations of motion. Furthermore this flow may be aptly referred to as the 'pure wall-flow' in the sense of Coles (1957), since the wake part of the mean velocity profile is absent there. These properties make the sink flow configuration a natural choice for the present systematic investigation of relationship between the large-scale structure and the pressure gradient. For a detailed account of sink flow turbulent boundary layers, the reader is referred to Jones, Marusic & Perry (2001) and Dixit & Ramesh (2008).

One of the common beliefs is that while outer layer is the one that primarily responds to the applied pressure gradient, inner layer remains largely universal (Coles 1956). Now in the case of sink flow turbulent boundary layers, it has been shown that as pressure gradient is made progressively more favourable, there is a concomitant shift of the mean velocity profile from the so-called universal log law (see Dixit & Ramesh 2008). Mean velocity profile in the overlap region is then describable by non-universal logarithmic laws where the parameters of these log laws become systematic functions of the pressure gradient parameter Δ_p (to be defined in § 3). Spalart & Leonard (1987), Nickels (2004) and Chauhan, Nagib & Monkewitz (2007) have also noted such non-universality in the log law for pressure-gradient-driven turbulent boundary layer flows. In view of this, it is natural to ask the question whether there are corresponding changes in the large-scale structure (in comparison with the

ZPG turbulent boundary layer) that are consistent with the observed non-universal behaviour of the inner region. This becomes the primary motivation for exploring large-scale structures in the present work. Furthermore, it appears that the structural details for reverse-transitional boundary layers have not been studied so far in the literature, and we attempt to do so in the present study within the framework of sink flow layers.

In the present paper, results of a systematic experimental investigation of some aspects of the large-scale structure in sink flow boundary layers are presented. The boundary layers under investigation are mostly turbulent except for the two cases that may be identified as being reverse transitional. The outline of the paper is as follows. Section 2 gives details of the experimental set-up and procedures used in the present work. This is followed in § 3 by the basic analysis of experimental data. This establishes conditions under which the present structural investigations are performed. Section 4 describes the main analysis of experimental data and the results pertaining to various aspects of the large-scale structure. Plausible structural models for sink flow turbulent boundary layers based on the present experimental results and the possibility of structural self-organization are also discussed therein. The phenomenon of relaminarization of a turbulent boundary layer by a strong streamwise FPG is examined from the structural viewpoint in the light of the present experimental results in § 5. The validity of Taylor's frozen turbulence hypothesis, as used in the present study, is examined in some detail in § 6. Section 7 gives details of the investigation of structure convection velocity and is followed by § 8 wherein conclusions are presented.

2. Experimental set-up and procedures

Experiments were carried out in an open-return wind tunnel (test-section size of 300 mm × 300 mm) at the Department of Aerospace Engineering, Indian Institute of Science. Details of the tunnel are given in Dixit & Ramesh (2008).

For the present investigations, the same experimental sink flow set-up, as described in Dixit & Ramesh (2008), was used (see figure 1*a*). Measurements were done at three different streamwise stations in the sink flow region with eight different pressure gradients investigated at each station. The pressure gradient was varied by changing the free-stream velocity in the test section. For measuring the wall-shear stress, the so-called surface hotwire (SHW) probe was used, which consists of a HW sensing element soldered to the tips of two sharp needles that protrude out from the surface of a Teflon plug which is fitted flush with the test surface. The height h of the sensing element from the wall was not measured directly but was estimated indirectly, from calibration of the SHW probe in ZPG flow (see Dixit & Ramesh 2008), to be approximately 60 μm (i.e. $h_+ = hU_\tau/\nu$ ranging from 0.62 to 3.57 over the entire range of experiments) so that the sensor always stayed in the viscous sublayer for all the flows under consideration. Here $U_\tau = \sqrt{\tau_w/\rho}$ is the friction velocity (τ_w is the wall-shear stress and ρ is the density of fluid) and ν is the kinematic viscosity of fluid. Further details of the SHW probe and its calibration can be found in Dixit & Ramesh (2008). Streamwise velocity was measured by a single HW probe.

Sensor elements for both the SHW and HW probes were Pt–Rh Wollaston wires with 5 μm core diameter. The active length l of the sensors was about 0.8 mm so that $l_+ = lU_\tau/\nu$ varied from 8 to 48 over the entire range of experiments. The length-to-diameter ratio (l/d) of the sensing elements was about 160 which was somewhat less than the usually recommended value of about 200 (Ligrani & Bradshaw 1987;

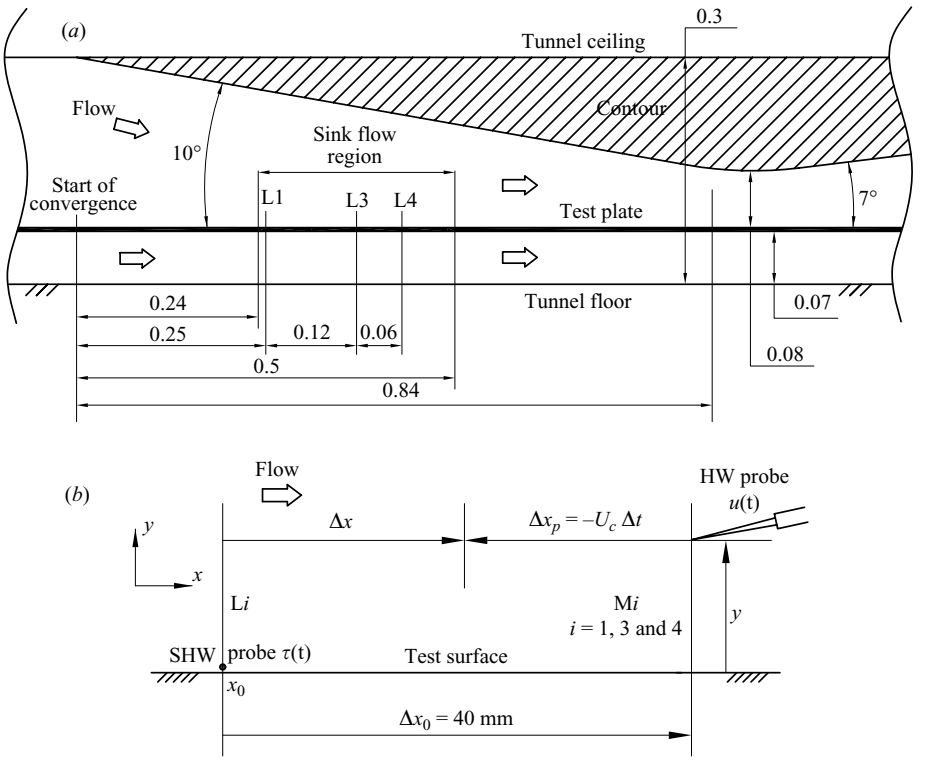

FIGURE 1. (*a*) Schematic of the experimental sink flow set-up. The figure is not to scale. All dimensions are in metres. (*b*) Side view of the probe arrangement used for measurement of the cross-correlation coefficient $R_{\tau u}(\Delta x, y)$.

Hutchins *et al.* 2009). This choice of l/d ratio was made to keep l_+ somewhat in control over the entire range of experiments. Very recently, Hutchins *et al.* (2009) have demonstrated that a reduction in the l/d ratio from 200 to 100 can cause serious attenuation of the streamwise turbulence intensity all across the boundary layer because of significant end conduction effects even though the l_+ values are acceptably low (about 22). In view of this, it was considered important to validate the performance of the present HW probe in a known flow. For this purpose, measurements were made with the same HW probe in a ZPG turbulent boundary layer flow having approximately the same Reynolds number ($R_\theta = 2843$) as that of the second flow ($R_\theta = 2900$) of DeGraaff & Eaton (2000). The measured turbulence intensity distribution showed excellent agreement all through the boundary layer with the corresponding intensity distribution from DeGraaff & Eaton (2000), which was measured using laser Doppler velocimetry (LDV). Thus it appears unlikely that the present use of the l/d ratio of about 160 can cause any serious problem.

Each sensor was operated by a constant-temperature HW anemometer manufactured by Sunshine Industries (Bangalore, India). Overheat ratio was kept at 1.5 for the HW sensor and 1.3 for the SHW sensor. Lower overheat ratio was used in the case of the SHW sensor to reduce conduction heat loss to the test surface. Fluctuating components of the signals from the SHW and the HW were amplified (amplification factor of 50) to improve the dynamical range. Signals were acquired using IOtech DaqBook (2000 series, 16 bit, 200 kHz; Data Acquisition System) and

the data acquisition software DASYLAB (version 7.0). Details regarding the sampling rate, duration and the like are given later in this section.

For the present study, the HW probe was located 40 mm downstream of the SHW probe in the same x–y plane where x is the streamwise coordinate and y is the wall-normal coordinate (see figure 1*b*). This choice of the spatial separation will be justified in § 6. Each measurement station is identified by the location of the SHW probe (L1, L3 and L4 in figure 1*a*), and eight different pressure gradients investigated at each station are denoted as PG1–PG8. Locations of the HW probe (40 mm downstream of each SHW probe) are denoted by M1, M3 and M4 respectively (not shown in figure 1*a*). The HW probe was traversed in the wall-normal direction using a dial-type height gauge (Mitutoyo, Japan) with a least count of 0.01 mm. Calibration of the HW probe was done *in situ* in the sink flow free stream where free-stream velocity U_∞ was known from the measured pressure distribution. Extensive measurements of friction velocity U_τ were done by Dixit & Ramesh (2008), and a complete mapping of U_τ over the entire sink flow region (stations L1–L5 in figure 2 from Dixit & Ramesh 2008) with various spatial locations and free-stream velocities was available from that study. Since the same set-up was used in the current work, the SHW probes in this study were calibrated *in situ* against those known values of U_τ (or τ_w). Signals from both the probes (HW and SHW) were acquired simultaneously with zero initial time delay. The spatial cross-correlation coefficient $R_{\tau u}(\Delta x, y)$ was obtained from these signals using Taylor's frozen turbulence hypothesis (Taylor 1938). The following discussion introduces relevant details of the procedure by which $R_{\tau u}(\Delta x, y)$ was obtained in course of the present work.

With $\tau\,(t)$ denoting the fluctuating wall-shear stress obtained from the SHW signal and $u\,(t)$ denoting the fluctuating streamwise velocity component obtained from the HW signal (see figure 1*b*), the spatio-temporal cross-correlation coefficient between $\tau\,(t)$ and $u\,(t)$, is defined as

$$R_{\tau u}\,(x_0,\, \Delta x_0,\, y,\, t_0,\, \Delta t) = \frac{\overline{\tau\,(x_0,\, t_0)\, u\,(x_0 + \Delta x_0,\, y,\, t_0 + \Delta t)}}{\sqrt{\overline{\tau^2}}\sqrt{\overline{u^2}}}. \tag{2.1}$$

Here the overbars denote long-time averages. In (2.1), x_0 is the location of the SHW sensor; Δx_0 is the streamwise spatial separation between the SHW and HW sensors ($\Delta x_0 > 0$ implies the HW downstream of the SHW); y is the wall-normal location of the HW sensor; t_0 is the initial time instant at which simultaneous acquisition of both the signals is started; and Δt is the time delay given to the $u\,(t)$ signal. Since we are presently studying statistically stationary turbulent signals, the initial time instant t_0 is insignificant and can be conveniently set to zero ($t_0 = 0$). Furthermore in the present study, Δx_0 is fixed at +40 mm. Therefore (2.1) may be written as

$$R_{\tau u}\,(x_0,\, y,\, \Delta t) = \frac{\overline{\tau\,(x_0)\, u\,(x_0 + \Delta x_0,\, y,\, \Delta t)}}{\sqrt{\overline{\tau^2}}\sqrt{\overline{u^2}}}. \tag{2.2}$$

Note that a positive time delay Δt given to the $u\,(t)$ signal amounts to moving upstream from the HW sensor by distance $\Delta x_p = -U_c \Delta t$ according to Taylor's frozen turbulence hypothesis (see figure 1*b*). Here Δx_p may be called the projection distance. Taylor's hypothesis assumes that the turbulence field convects downstream without appreciable distortion, and hence a time series obtained from a point probe may be converted to a space series using the transformation

$$x_p = -U_c t \quad \text{or} \quad \Delta x_p = -U_c \Delta t, \tag{2.3}$$

where $U_c = U_c(y)$ is the local convection velocity. The space series so obtained may be considered to be a one-dimensional slice through the turbulence field for the particular fluctuating quantity under consideration. With Taylor's hypothesis applied, the $u(t)$ signal at $(x_0 + \Delta x_0)$ with a time delay of Δt is equivalent to the $u(t)$ signal at $(x_0 + \Delta x_0 + \Delta x_p)$ with zero time delay ($\Delta t = 0$). If we denote $(\Delta x_0 + \Delta x_p)$ by Δx as shown in figure 1(*b*), then (2.2) may be rewritten as

$$R_{\tau u}(x_0, \Delta x, y) = \frac{\overline{\tau(x_0)\, u(x_0 + \Delta x, y)}}{\sqrt{\overline{\tau^2}}\sqrt{\overline{u^2}}}. \tag{2.4}$$

Notice that Δx_p is by definition negative (for a positive time delay Δt) and therefore $\Delta x < \Delta x_0$ (see figure 1*b*). Thus Taylor's hypothesis enables surrogate estimation of the spatial cross-correlation coefficient from the time-series data; the validity of Taylor's hypothesis has been investigated and confirmed experimentally for the present measurements as discussed further in § 6. It is clear that as the time delay Δt in the HW signal is progressively increased, one moves to increasingly larger distances upstream of the HW, i.e. closer to the SHW. Figure 1(*b*) clarifies the nomenclature used in the above-given discussion. In what follows we shall call the spatial cross-correlation coefficient $R_{\tau u}(x_0, \Delta x, y)$ simply the cross-correlation coefficient $R_{\tau u}(\Delta x, y)$ unless stated otherwise.

For the convenience of discussion, only positive time delay has been discussed above. It is however clear that a negative time delay may as well be given to the HW signal that would project it downstream of the HW probe. Such a delay would thus give information about $R_{\tau u}(\Delta x, y)$ downstream of the HW. In the present work, both types of delays have been used to derive information about the large-scale structure.

In the present study, both the HW and the SHW were calibrated, and therefore fluctuating voltage signals from them were converted to corresponding fluctuating quantities. To assess the linearization approximation involved in such a conversion, the following exercise was carried out. Root-mean-squared (r.m.s.) values of the streamwise velocity fluctuation $u(t)$ and the wall-shear stress fluctuation $\tau(t)$ were calculated (*a*) by applying appropriate King's laws to the instantaneous voltage signals to obtain instantaneous quantities and then subtracting out the mean from them and (*b*) by directly using linearization approximation to obtain fluctuating quantities from the corresponding fluctuating voltages. It was found that for the weakest pressure gradient PG1 (i.e. the highest-Reynolds-number case in the present study), typical differences between the r.m.s. values of both $u(t)$ and $\tau(t)$ obtained by the above two methods were of the order of 3 % each. For the strongest pressure gradient PG8 (i.e. the lowest-Reynolds-number case in the present study), these differences were found to be about 6 % and 10 % respectively. Given that the r.m.s. values of $u(t)$ and $\tau(t)$ are an order of magnitude smaller in the case of PG8 than in the case of PG1, higher percentage differences in the PG8 case are not as severe as they appear. In view of this, it was decided to use the linearization approximation in the present study. This implied that the calculation of $R_{\tau u}(\Delta x, y)$ may be carried out simply with the fluctuating voltages, since the constants of proportionality would cancel out from the numerator and the denominator. It was confirmed from the measured data that this indeed was the case. Therefore in this study, all values of $R_{\tau u}(\Delta x, y)$ have been obtained by directly correlating the fluctuating voltages from both the sensors.

The main requirement in an investigation involving measurement of $R_{\tau u}(\Delta x, y)$ is to ensure its convergence. If the total sampling duration is sufficiently long, then the time averaging involved in evaluation of $R_{\tau u}(\Delta x, y)$ takes into account sufficiently large

	U_∞ ms^{-1}					
Flow code	M1	M3	M4	T (s)	f_s (kHz)	f_{kmax} at M4 (kHz)
PG1	16.66	18.68	19.93	60	10	3.08
PG2	13.93	15.44	16.30	60	10	2.80
PG3	10.88	12.04	12.69	90	6	1.83
PG4	7.32	8.42	8.80	90	6	1.08
PG5	5.95	6.74	6.93	120	4	0.65
PG6	4.46	4.91	5.12	120	4	0.31
PG7	3.54	3.93	4.23	160	3	0.17
PG8	2.82	3.33	3.43	160	3	0.08

TABLE 1. Sampling parameters adjusted for the variation in the free-stream velocity over the entire range of experiments: U_∞ is the free-stream velocity; T is the sampling duration; f_s is the sampling rate; and f_{kmax} is the maximum Kolmogorov frequency scale.

number of organized activities, and this stabilizes the limiting value of $R_{\tau u}(\Delta x, y)$. For higher free-stream velocities, large number of organized activities are convected over the sensors in a relatively short time, and therefore relatively smaller sampling duration may be sufficient to ensure adequate convergence of $R_{\tau u}(\Delta x, y)$. However if the free-stream velocity is reduced (as is done in the present study to alter the pressure gradient), larger sampling duration is required for averaging over, say, the same number of organized activities. Thus the sampling duration needs to be adjusted for the free-stream velocity variation to ensure adequate convergence of $R_{\tau u}(\Delta x, y)$. Furthermore, as the free-stream velocity reduces, the Reynolds number of the sink flow boundary layer comes down (in the present study), and the corresponding Kolmogorov frequency scale f_k (reciprocal of the Kolmogorov time scale $t_k = (\nu/\epsilon)^{1/2}$, where ϵ is the dissipation rate of turbulence kinetic energy in kinematic units) decreases. This permits appropriate reduction in the sampling rate with reduction in the free-stream velocity. To summarize, with the reduction in free-stream velocity the sampling duration should increase, and the sampling rate may be decreased appropriately.

Table 1 gives the sampling parameters along with the corresponding free-stream velocities for all the eight pressure gradients (PG1–PG8) at all the three measurement stations. It was found that a sampling duration of $T = 20$ s was sufficient to yield well-converged values of $R_{\tau u}(\Delta x, y)$ for flow PG1 (this roughly corresponds to about 20 000 boundary layer turnover times, i.e. $TU_\infty/\delta = 20\,000$). This implies that for PG8 if averaging is to be done, say, over the same number of organized activities as in PG1, sampling duration T should be about 116 s (provided that the boundary layer thicknesses are not very different; see table 2). Table 1 indicates that the actual values of sampling duration used are larger than the above-mentioned values. This therefore ensures adequate convergence of the values of $R_{\tau u}(\Delta x, y)$ in all flows in the present study.

Also given in table 1 are the estimates of the maximum Kolmogorov frequency scale f_{kmax} (which is the reciprocal of the minimum Kolmogorov time scale t_{kmin}) at HW station M4. These are obtained from the dissipation estimates calculated from one-dimensional power-density spectra; typical power-density spectra are shown in the next section. Even though such estimates of dissipation are known to be somewhat erroneous in the immediate vicinity of the wall because of anisotropy effects, their use in the present context is meant only as a rough guideline (see Ligrani & Bradshaw 1987). It may be seen from table 1 that the Nyquist criterion is well satisfied for all

HW probe at M1

Flow	$K \times 10^6$	U_∞ (ms^{-1})	C_f	Δ_p	δ (mm)	R_{δ^*}	R_θ	H
PG1	0.77	16.66	0.00410	−0.00830	16.37	1731	1301	1.33
PG2	0.95	13.93	0.00398	−0.01065	16.69	1683	1248	1.35
PG3	1.23	10.88	0.00403	−0.01360	17.20	1191	901	1.32
PG4	1.74	7.32	0.00469	−0.01533	18.14	853	597	1.43
PG5	2.18	5.95	0.00468	−0.01928	15.84	755	510	1.48
PG6	2.90	4.46	0.00492	−0.02373	18.22	613	396	1.55
PG7	3.55	3.54	0.00564	−0.02371	15.14	445	279	1.60
PG8	4.52	2.82	0.00603	−0.02734	16.25	370	219	1.69

HW probe at M3

Flow	$K \times 10^6$	U_∞ (ms^{-1})	C_f	Δ_p	δ (mm)	R_{δ^*}	R_θ	H
PG1	0.77	18.68	0.00405	−0.00847	14.93	1760	1325	1.33
PG2	0.95	15.44	0.00399	−0.01062	15.08	1490	1099	1.36
PG3	1.23	12.04	0.00400	−0.01371	15.77	1236	883	1.40
PG4	1.74	8.42	0.00423	−0.01793	16.04	909	646	1.41
PG5	2.18	6.74	0.00428	−0.02205	16.63	702	476	1.48
PG6	2.90	4.91	0.00464	−0.02592	17.87	597	387	1.54
PG7	3.55	3.93	0.00511	−0.02753	14.64	418	250	1.67
PG8	4.52	3.33	0.00467	−0.04002	15.42	402	236	1.71

HW probe at M4

Flow	$K \times 10^6$	U_∞ (ms^{-1})	C_f	Δ_p	δ (mm)	R_{δ^*}	R_θ	H
PG1	0.77	19.93	0.00402	−0.00857	13.71	1769	1318	1.34
PG2	0.95	16.30	0.00404	−0.01043	14.75	1524	1125	1.35
PG3	1.23	12.69	0.00405	−0.01346	15.53	1196	876	1.37
PG4	1.74	8.80	0.00434	−0.01723	15.84	868	613	1.42
PG5	2.18	6.93	0.00453	−0.02024	16.04	655	439	1.49
PG6	2.90	5.12	0.00474	−0.02513	16.34	553	352	1.57
PG7	3.55	4.23	0.00489	−0.02942	13.57	420	255	1.65
PG8	4.52	3.43	0.00486	−0.03774	14.70	380	223	1.71

TABLE 2. Various parameters associated with the mean velocity profiles at all the three HW locations M1, M3 and M4.

the cases (i.e. $f_s > 2 \times f_{kmax}$). Further since large-scale structure is the focus of the present study, capturing the low- and moderate-wavenumber parts of the spectrum is more relevant in the present context. Table 1 thus confirms that the sampling rates used in the present study are quite adequate.

3. Basic analysis of the experimental data

Mean velocity profiles in the present study were measured by the HW probe located 40 mm downstream of the SHW probe (HW probe locations M1, M3 and M4). For plotting these profiles in inner coordinates (i.e. U_+ versus y_+), friction velocities U_τ at the HW locations are required for all pressure gradients. As mentioned before in the previous section, a complete mapping of U_τ with various spatial locations and free-stream velocities in the sink flow region was available from the previous study of Dixit & Ramesh (2008). This information was used to get values of U_τ at all the three HW locations M1, M3 and M4 by interpolation, since the present HW locations lie between the SHW locations. Table 2 gives the details of parameters associated with the

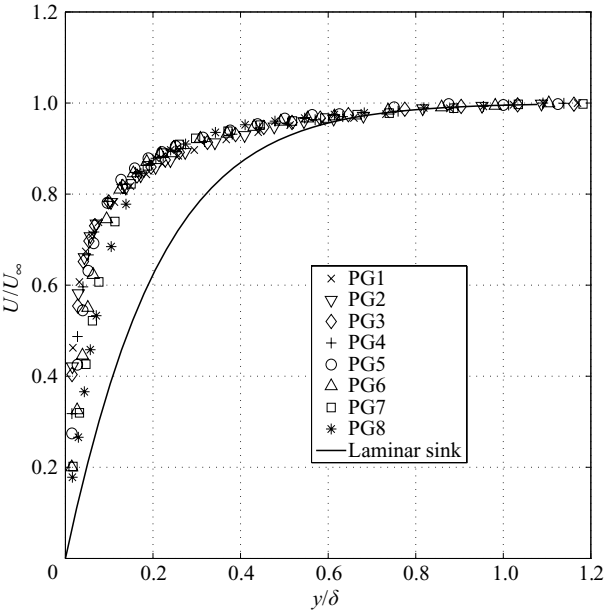

FIGURE 2. Mean velocity profiles at HW station M4 in conventional coordinates for different pressure gradients in the present study.

mean velocity profiles at all the three HW locations. In table 2, U_∞ is the free-stream velocity; δ is the boundary layer thickness based on 99.5 % of U_∞; $C_f = 2(U_\tau/U_\infty)^2$ is the skin friction coefficient; $K = (\nu/U_\infty^2)\,\mathrm{d}U_\infty/\mathrm{d}x$ is the acceleration parameter; and $\Delta_p = (\nu/\rho U_\tau^3)\,\mathrm{d}p/\mathrm{d}x$ is the pressure gradient parameter. Further, R_θ is the Reynolds number based on momentum thickness θ; R_{δ^*} is the Reynolds number based on displacement thickness δ^*; and $H = \delta^*/\theta$ is the conventional shape factor.

The attainment of asymptotic sink flow state is characterized by the streamwise constancy exhibited by parameters K, C_f, Δ_p, H and all the Reynolds numbers (see Jones *et al.* 2001; Dixit & Ramesh 2008). It was noted in Dixit & Ramesh (2008) that in the present sink flow set-up, mean flow was very close to the asymptotic state at and downstream of station L3. In the present context where measurements have been done at L1, L3 and L4, this implies that the flow at L1 has not quite attained the asymptotic state, while that at L3 and L4 is very close to the asymptotic state. Values of parameters in table 2 reconfirm this observation.

Figure 2 shows mean velocity profiles at HW station M4 in conventional coordinates (i.e. U/U_∞ versus y/δ) for different pressure gradients. Also plotted is the laminar sink flow solution which is an exact solution (see Schlichting & Gersten 2000). The profiles corresponding to pressure gradients PG7 and PG8 appear to be reverse transitional, since they are less full compared with other profiles and show progressive shift towards the laminar solution. It is difficult to identify and quantify the precise conditions that define onset of reverse transition, since it is supposed to be a gradual process (see Narasimha & Sreenivasan 1973, 1979; Sreenivasan 1982). Therefore certain arbitrariness is bound to exist while identifying certain turbulent boundary layers in the present study as being reverse transitional.

Figure 3 shows the same mean velocity profiles of figure 2 in inner coordinates (i.e. U_+ versus y_+). Clearly all profiles show significant departures from the universal logarithmic law as is well known in the case of strong-FPG turbulent boundary layer

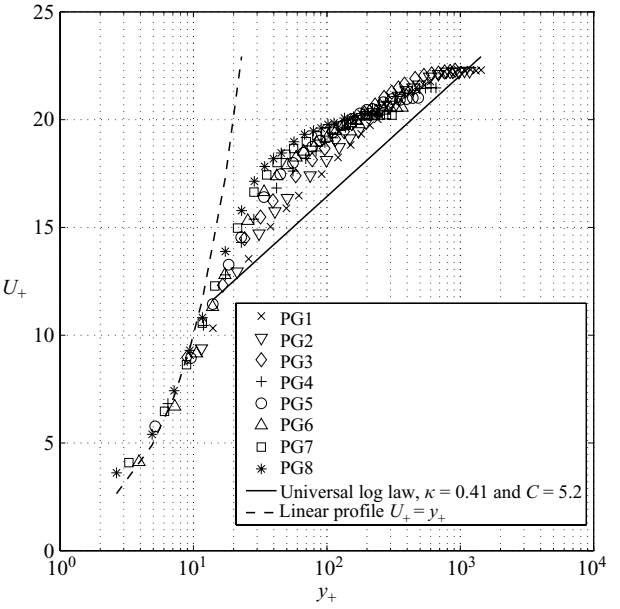

FIGURE 3. Mean velocity profiles at HW station M4 in inner coordinates for different pressure gradients in the present study.

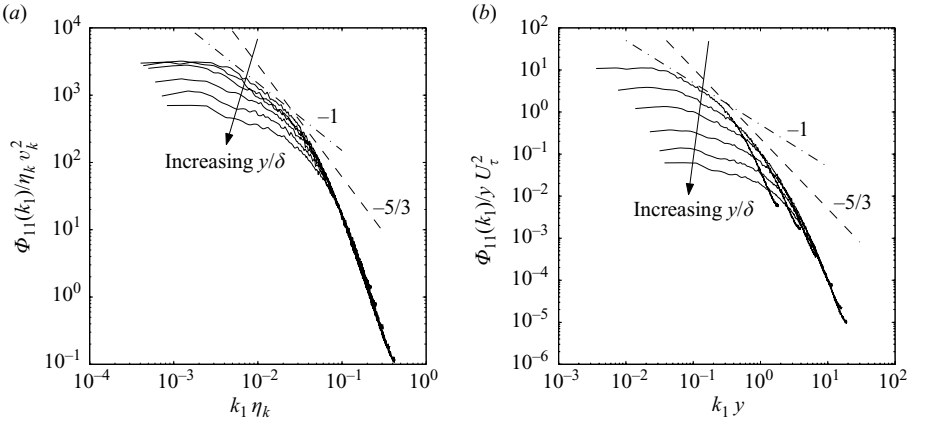

FIGURE 4. One-dimensional power-density spectra for flow PG1 with the HW at station M4 in (*a*) the Kolmogorov scaling and (*b*) the wall or inner scaling; y/δ values are 0.06, 0.15, 0.29, 0.51, 0.73 and 0.88; —·—, k_1^{-1} law scaling; ——, $k_1^{-5/3}$ law scaling.

flows (see Dixit & Ramesh 2008). It is seen that the viscous sublayer occupies increasingly larger fractions of the total boundary layer thickness as the FPG becomes severer. This is evident from the progressive shift of near-wall velocity profiles ($y_+ < 20$) towards the linear velocity profile $U_+ = y_+$. Figure 3 corroborates the inference regarding the reverse-transitional nature of PG7 and PG8 profiles drawn from figure 2 in the preceding paragraph.

Figure 4 shows typical power-density spectra for case PG1 at HW station M4 for various wall-normal locations in the Kolmogorov scaling and the wall or inner scaling.

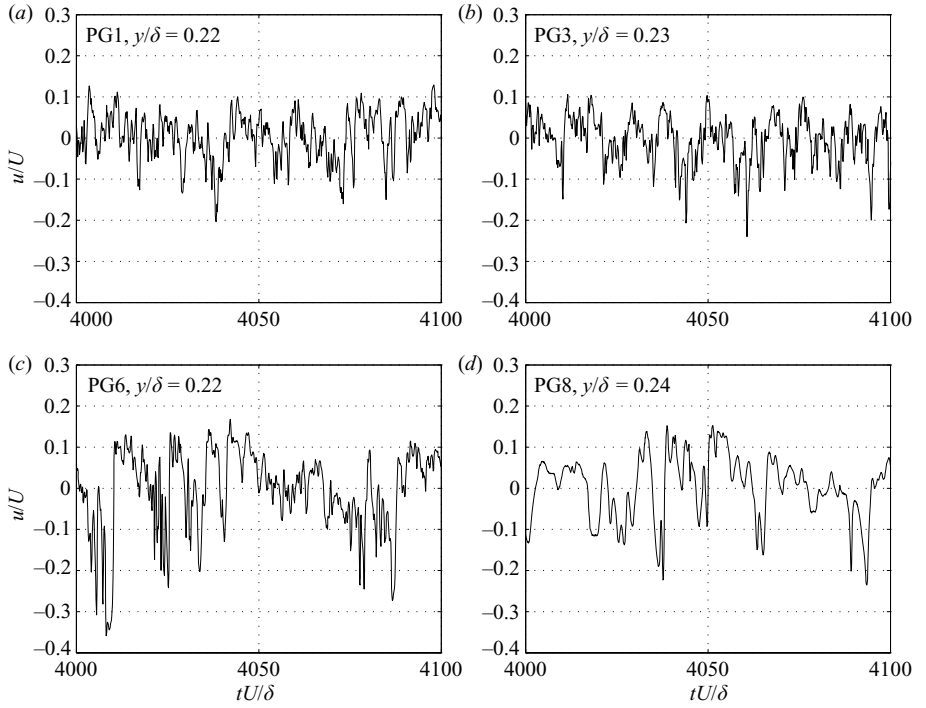

FIGURE 5. Typical time traces of the streamwise fluctuating velocity at y/δ of approximately 0.23 for pressure gradients PG1, PG3, PG6 and PG8. HW station is M4. Local mean velocity U and boundary layer thickness δ are used for non-dimensionalization.

Here the wavenumber power spectral density $\phi_{11}(k_1)$ is defined from the relation

$$\overline{u^2} = \int_0^\infty \phi_{11}(k_1)\,\mathrm{d}k_1, \tag{3.1}$$

where $\overline{u^2}$ is the mean-squared streamwise velocity fluctuation and k_1 is the streamwise wavenumber. Conversion from frequency f to wavenumber k_1 is done using Taylor's hypothesis with convection velocity taken to be equal to the local mean velocity U, i.e. $k_1 = 2\pi f/U$. The Kolmogorov length, time and velocity scales, denoted respectively by η_k, t_k and v_k, are defined in the usual fashion (see Tennekes & Lumley 1972). It may be noted in figure 4(a) that the high-wavenumber ends of all the spectra at different heights across the boundary layer collapse well in the Kolmogorov scaling as expected (see Saddoughi & Veeravalli 1994). Also it may be seen from figure 4(b) that the spectra in the inner scaling collapse fairly well beyond $k_1 y = 1$ approximately, except for the lowest y/δ spectrum. This indicates that the wall scaling for spectra prevails, beyond the wavenumbers given by the inverse of the wall-normal distance, almost all through the boundary layer as may be expected in the case of sink flows (i.e. pure wall-flows according to Coles 1957). The Reynolds number is perhaps too low to observe a substantial region of universal equilibrium scaling, i.e. the $k_1^{-5/3}$ law. There appears to be a small region of k_1^{-1} law, especially for the near-wall spectra. However this region is also too small to make any conclusive statement.

Figure 5 shows typical time traces of the normalized fluctuating velocity, i.e. $u(y,t)/U(y)$, for pressure gradients PG1, PG3, PG6 and PG8 at HW location M4. All the traces correspond to the same wall-normal location having y/δ of about

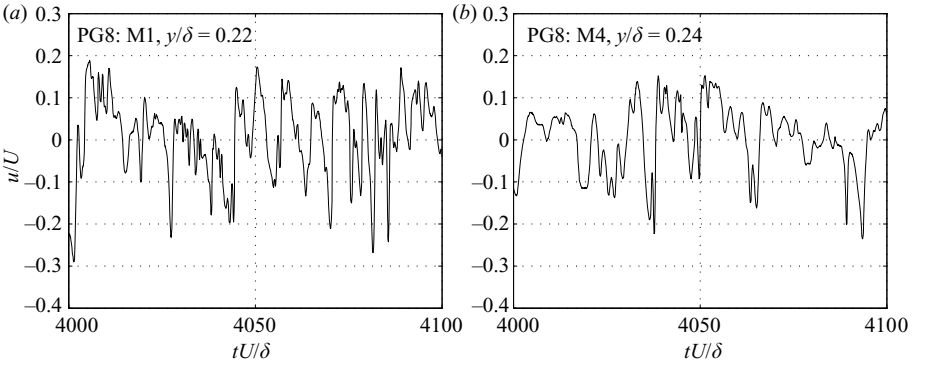

FIGURE 6. Comparison of time traces of the streamwise fluctuating velocity at HW stations M1 and M4 and at the same y/δ (about 0.23) for pressure gradient PG8. Local mean velocity U and boundary layer thickness δ are used for non-dimensionalization.

0.23. Time axis has been non-dimensionalized by the local mean velocity U and the boundary layer thickness δ. Time traces for PG1 and PG3 show considerable high-frequency activity, whereas those for PG6 and PG8 clearly show progressive reduction in the high-frequency content. Furthermore the signals become progressively spiky and negatively skewed (large excursions on the negative side of u/U axis) as the FPG is increased. These observations support the contention of figures 2 and 3 that flows PG7 and PG8 are reverse transitional.

Figure 6 shows a comparison of time traces of the streamwise velocity fluctuation obtained at same y/δ (about 0.23) at HW stations M1 and M4 for flow PG8. It is apparent that the signal at M1 is richer in terms of its frequency content as compared with the signal at the downstream station M4. This is indicative of the fact that the flow which is initially turbulent is approaching a reverse-transitional state, and thus this observation also supports the contention regarding the reverse-transitional nature of PG8.

Figure 7 shows comparison of the mean velocity profiles in the present study obtained by HW anemometry with the Pitot-tube measurements of an earlier study by Dixit & Ramesh (2008) for the same pressure gradient PG2 (PE2 in Dixit & Ramesh 2008) in the same experimental sink flow set-up. The excellent agreement, seen in figure 7, serves as a check on the quality and consistency of the present measurements.

Figure 8 shows the reverse-transitional mean velocity profiles at streamwise stations M3 and M4 for pressure gradient PG8 in the conventional (i.e. laminar-like) and inner scalings respectively. The excellent collapse seen in figure 8 is somewhat surprising and in fact quite interesting, since reverse-transitional profiles are expected to be in a non-equilibrium evolving state and are not expected to conform to the laminar-like or inner law scalings. This interesting result, however, needs to be slightly tempered with caution, as the streamwise separation between locations M3 and M4 is only about 4δ, where δ is the typical boundary layer thickness in the present study. Even so, we believe that this result is likely to hold for larger streamwise separations also. In view of this, the sink flow configuration presents a really attractive framework for exploring reverse transition in greater detail. This possibility of using sink flow to effectively study relaminarization appears to have been anticipated by Sreenivasan (1981).

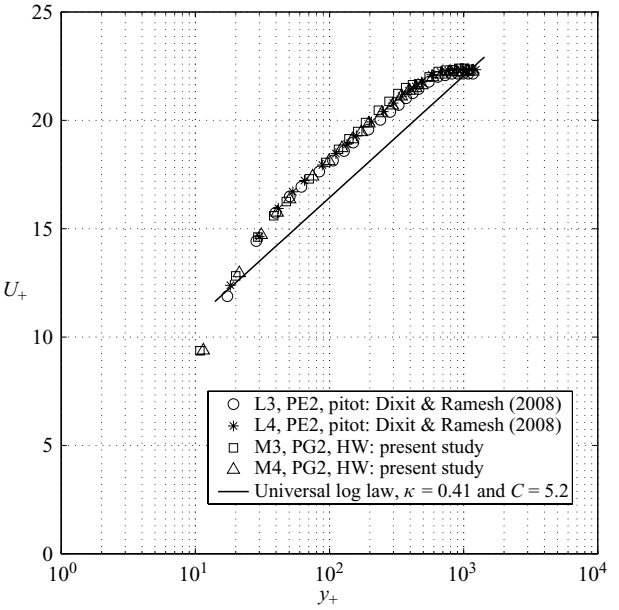

FIGURE 7. Consistency check between the present HW study and the Pitot-tube study by Dixit & Ramesh (2008). Comparison of mean velocity profiles for the same pressure gradient.

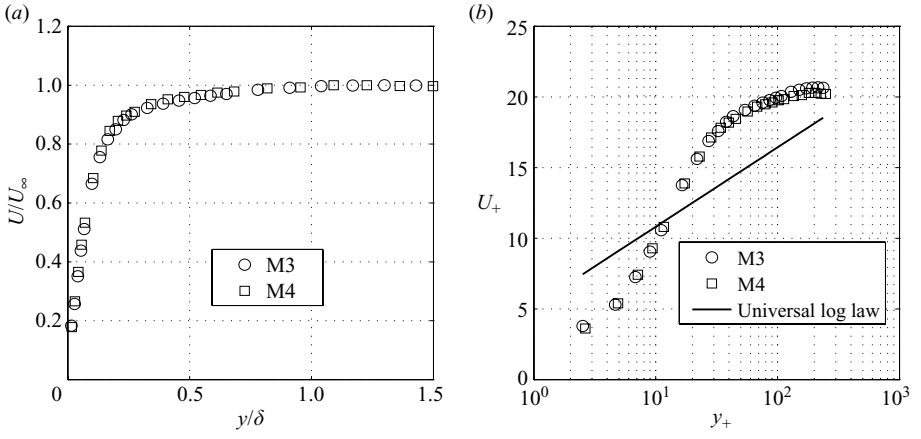

FIGURE 8. Streamwise collapse of reverse-transitional profiles in (*a*) conventional coordinates and (*b*) inner coordinates. Pressure gradient is PG8.

4. Investigation of the large-scale structure

4.1. *Typical cross-correlation coefficient* $R_{\tau u}(\Delta x, y)$ *curves*

For obtaining the orientation or inclination of the large-scale structure experimentally, the cross-correlation coefficient $R_{\tau u}(\Delta x, y)$ between the fluctuating wall-shear stress $\tau(t)$ and the streamwise velocity fluctuation $u(t)$ was measured. The probe arrangement (figure 1*b*) has already been discussed in § 2. The HW probe was located 40 mm downstream of the SHW probe and was traversed in the wall-normal direction. The positive or negative time delay (Δt) given to the HW signal was converted to spatial distance upstream or downstream of the HW ($\Delta x_p = -U_c \Delta t$) by

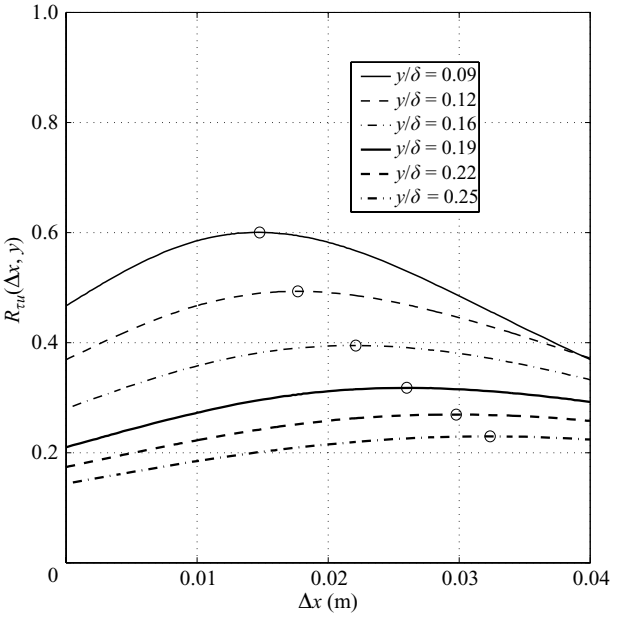

FIGURE 9. Typical cross-correlation coefficient $R_{\tau u}(\Delta x, y)$ curves obtained using Taylor's hypothesis applied to the HW signal for pressure gradient PG6. The SHW is at L4 ($\Delta x = 0$), and the HW is at M4 ($\Delta x = 0.04$ m). The circles mark the maximum of $R_{\tau u}(\Delta x, y)$ at a given y-location, and the corresponding value of Δx will be denoted by Δx_{max} for that y-location.

making use of Taylor's hypothesis. Convection velocity in Taylor's hypothesis was taken to be the same as the local mean velocity (i.e. $U_c(y) = U(y)$). The validity of Taylor's hypothesis and the choice of convection velocities in the present study are discussed later in greater detail in §§ 6 and 7 respectively.

Figure 9 shows the typical cross-correlation coefficient $R_{\tau u}(\Delta x, y)$ curves obtained using Taylor's hypothesis applied to the HW signal for pressure gradient PG6. Note that as one moves away from the wall, (i) the peak value of $R_{\tau u}(\Delta x, y)$ decreases (i.e. the correlation becomes weak), and (ii) the peak moves away from the SHW location in the downstream direction. The second observation indicates the presence of a large-scale structure that is leaning forward in the direction of the flow.

4.2. *Orientation of the large-scale structure in pressure gradients*

Identification of the structure involves locating the maximum of $R_{\tau u}(\Delta x, y)$ spatially, i.e. to find the distance $\Delta x = \Delta x_{max}$ (see figures 1*b* and 9) downstream of the SHW where $R_{\tau u}(\Delta x, y)$ reaches its maximum for a given y-location. In the present study, for a given y-location, the maximum of $R_{\tau u}(\Delta x, y)$ was first located upstream or downstream of the HW probe (i.e. Δx_{pmax} was obtained) by applying Taylor's hypothesis to the HW signal. This distance Δx_{pmax} was then converted to distance Δx_{max} downstream of the SHW probe using the relation $\Delta x_{max} = \Delta x_0 + \Delta x_{pmax}$ (see figure 1*b*). Note that $\Delta x_{pmax} < 0$ if the peak in $R_{\tau u}(\Delta x, y)$ occurs upstream of the HW and $\Delta x_{pmax} > 0$ if it occurs downstream. This exercise was carried out over the entire thickness of the boundary layer for all pressure gradients. The plot of distance y from the wall versus distance Δx_{max} corresponding to the maximum of $R_{\tau u}(\Delta x, y)$ was then constructed (see figure 10). The local structure inclination angle $\alpha(y)$ is defined

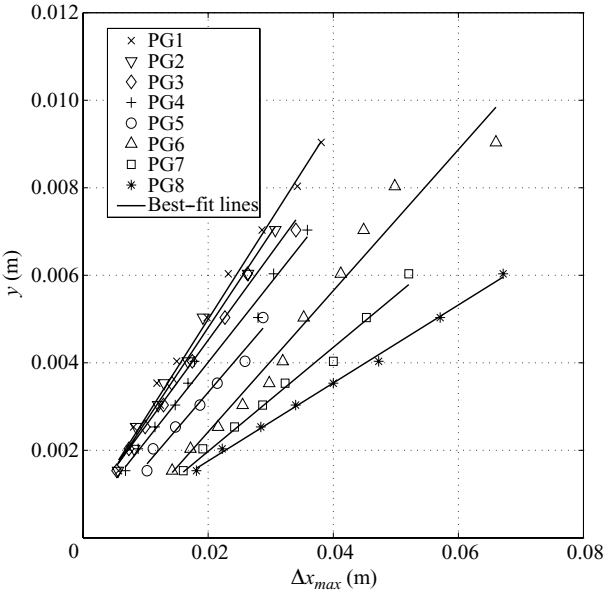

FIGURE 10. Variation of the average structure inclination angle α_{avg} with pressure gradient. The SHW is at L4, and the HW is at M4. Slope of each best-fit line gives α_{avg} from (4.2).

as the inverse tangent of the local slope of y versus Δx_{max} plot, i.e.

$$\alpha(y) = \tan^{-1}\left(\left.\frac{\mathrm{d}y}{\mathrm{d}\Delta x_{max}}\right|_{y}\right). \tag{4.1}$$

It was found that within the experimental scatter, y is a linear function of Δx_{max} to a good approximation, for a range of y values for all pressure gradients. This observation enabled the definition of average structure inclination α_{avg} as the inverse tangent of the slope of the best-fit line (least squares method) over that range of y values:

$$\alpha_{avg} = \tan^{-1}\left(\left.\frac{\mathrm{d}y}{\mathrm{d}\Delta x_{max}}\right|_{\text{best-fit}}\right). \tag{4.2}$$

Figure 10 shows the y versus Δx_{max} plot at SHW location L4 (and therefore the HW is at M4) for all the pressure gradients under consideration. The best-fit lines (least squares method) are also shown. Here onwards in the current paper, the phrase 'structure angle' would mean 'average structure inclination angle α_{avg}'. It is already noted (see figure 9) that the maximum value of $R_{\tau u}(\Delta x, y)$ decreases away from the wall. It was also observed that the smallest well-defined value of the peak in $R_{\tau u}(\Delta x, y)$ that could be located unambiguously was about 0.1. Therefore points in figure 10 do not extend beyond $y = 9$ mm approximately, since beyond this wall-normal location, the peak in $R_{\tau u}(\Delta x, y)$ was not well defined and unambiguous.

The most important observation that is evident from figure 10 is that there is a systematic trend in the structure angle as the pressure gradient is varied; α_{avg} decreases systematically and the structure becomes flatter as one goes on increasing the strength of the FPG.

At this stage, it is important to emphasize the following connection which concerns the primary motivation of the present study as mentioned in § 1. It has been shown here, perhaps for the first time in the literature on accelerating turbulent boundary

layers in general and sink flows in particular, that there exists a systematic trend of orientation of the large-scale structure with strength of the pressure gradient as seen in figure 10. In an earlier study of the mean velocity scaling by Dixit & Ramesh (2008) in the same sink flow set-up, it was observed that the logarithmic law exhibited by a sink flow turbulent boundary layer undergoes systematic variations with the pressure gradient (the non-universal, pressure-gradient-dependent log laws). It therefore appears that it would not be inappropriate to educe the structural behaviour that is consistent with the observed mean velocity scaling.

Another important aspect that deserves discussion is the possible Reynolds number dependence of the structure inclination. The present experiments have $R_\tau = \delta U_\tau/\nu = \delta_+$ values ranging from about 816 for PG1 to about 166 for PG8 at station M4. This was somewhat unavoidable, since pressure gradient in the present study was varied by changing the free-stream speed, which resulted in change of the Reynolds number of the sink flow. Therefore in the present results there could very well have been a combined effect of both the pressure gradient and the Reynolds number. In order to rule out the possibility of any substantial Reynolds number dependence, it is instructive to take a closer look at the available ZPG results at different Reynolds numbers.

Adrian *et al.* (2000) have covered the range of Reynolds numbers $R_\tau = 355$–2000 for ZPG turbulent boundary layers. Though their results pertain to the instantaneous packet inclinations, they have not reported any discernible Reynolds number dependence of the structure inclination (say at a fixed value of y_+). Linear stochastic estimations of Christensen & Adrian (2001) for turbulent channel flows have shown that the averaged packet inclinations (of about 12°) are almost the same for the two different Reynolds numbers, $R_\tau = 547$ and 1734, studied. In a recent DNS study, Lee & Sung (2009) have also reported very similar instantaneous and average packet inclinations in a ZPG layer (R_τ of about 600–700) as Adrian *et al.* (2000) and Christensen & Adrian (2001). Marusic & Heuer (2007) have shown that the structure inclination (of about 13°–15°), measured by cross-correlation studies in ZPG turbulent boundary layer flows, is remarkably invariant over almost three decades of the Reynolds number R_τ ranging from 10^3 to 10^6 (i.e. moderate to large). There appear to be no other systematic studies in the case of ZPG turbulent boundary layers that investigate or compare structure inclinations over a range of Reynolds numbers from low to moderate and high values. Further it is conceivable that the dominant Reynolds number effect in a low-Reynolds-number ZPG flow is that the vortices would not be as compact (i.e. more diffused) as in a high-Reynolds-number flow. It is however difficult to see how such an effect would alter the packet inclinations significantly. Therefore in view of the available results from Adrian *et al.* (2000), Christensen & Adrian (2001), Lee & Sung (2009) and Marusic & Heuer (2007) it appears reasonable to expect that the Reynolds number effects in the present study would be negligible in comparison with the pressure gradient effects. In addition, as mentioned in Dixit & Ramesh (2008), use of Δ_p as the reference for comparing structure inclinations in the present study (see § 4.3) may be viewed as a means to account for the Reynolds number indirectly through C_f which is present in the definition of Δ_p.

4.3. *Streamwise variation of the structure angle*

Since experiments were performed in the present study at three streamwise stations (the SHW at L1, L3 and L4 and the corresponding HW at M1, M3 and M4 respectively), it is natural to compare the structure angle results for these stations. In particular it is of interest to see whether the structure angle also reaches its

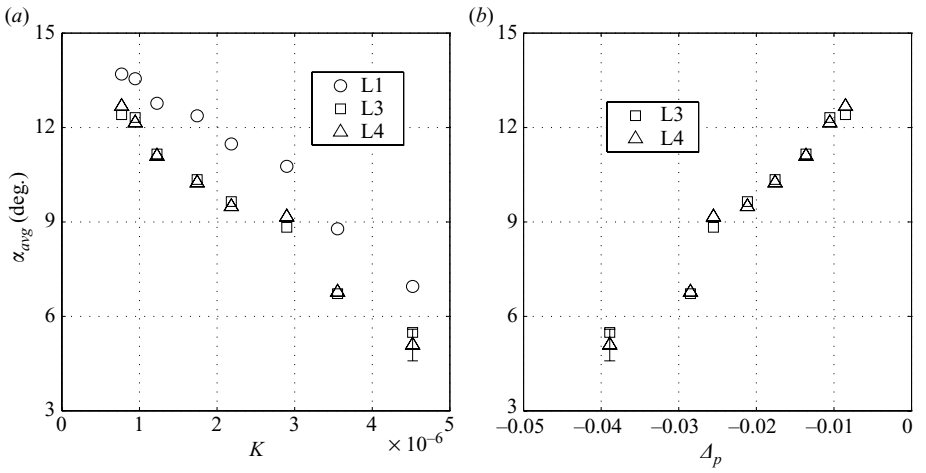

FIGURE 11. Variation of the structure angle α_{avg} plotted against (a) the acceleration parameter K (for stations L1, L3 and L4) and (b) the pressure gradient parameter Δ_p (for stations L3 and L4). Typical uncertainty of $\pm 0.5^\circ$ in α_{avg} is also indicated.

asymptotic value in the sink flow configuration as do the other flow parameters such as the Reynolds numbers and skin friction coefficient (see Dixit & Ramesh 2008).

In the first place, it is necessary to decide on an appropriate measure of the streamwise pressure gradient. The acceleration parameter $K = (\nu/U_\infty^2)\,\mathrm{d}U_\infty/\mathrm{d}x$ depends purely on the free-stream velocity U_∞ (for a given fluid) and reaches a constant value just before station L1 (see Dixit & Ramesh 2008 and figure 1a of the current paper). Thus as far as K is concerned, stations L1, L3 and L4 all belong to the $K =$ constant region. However it is noted in Dixit & Ramesh (2008) that the boundary layer (mean flow) parameters such as the Reynolds numbers and skin friction coefficient C_f reach close to their asymptotic values just before station L3. Therefore the pressure gradient parameter $\Delta_p = -K/(C_f/2)^{3/2}$ attains a nearly constant value just before station L3. Thus it appears appropriate to use K as the measure of pressure gradient when structure angles at all the three stations are being compared. On the other hand, Δ_p is more relevant when results at and downstream of L3 are being compared.

Figure 11(a) shows the variation of structure angle α_{avg} with the acceleration parameter K for all the three streamwise measurement stations. Within the experimental uncertainty, there is remarkable agreement between the values of α_{avg} at stations L3 and L4 for all pressure gradients. It has been noted previously that the mean flow at and downstream of station L3 is in a state that is very close to the asymptotic sink flow state. Therefore it appears that the structure inclination indeed approaches its asymptotic value in the asymptotic sink flow configuration. The values of α_{avg} at L1 are consistently higher for all pressure gradients, indicative of the adjustment that is needed before the flow comes close to the asymptotic state at L3. Figure 11(b) shows the structure angle variation with the pressure gradient parameter Δ_p for stations L3 and L4. Also note that the extrapolation of the trend of structure angle variation in figure 11 to the ZPG case (i.e. $K = 0$ or $\Delta_p = 0$) yields $\alpha_{avg} = 14^\circ$ approximately, which is consistent with the ZPG data in the literature (see § 1).

It may be noted in figure 11 that initially when the FPG is weak, structure angle decreases rapidly with the increase in the FPG. As the FPG is progressively made severe, the rate of decrease of structure angle reduces till a critical value corresponding

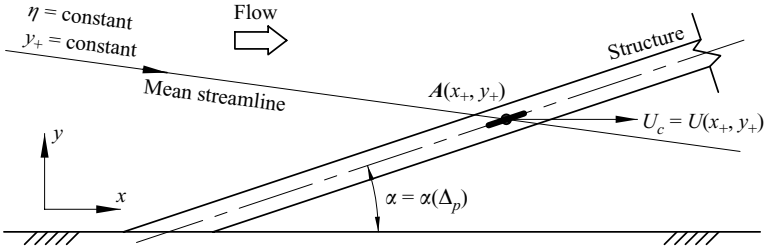

FIGURE 12. Streamwise constancy of the structure angle in a sink flow boundary layer. The thick solid line at $\boldsymbol{A}$ represents infinitesimal length of the structure around $\boldsymbol{A}$. Coordinates of $\boldsymbol{A}$ are shown in the inner scaling.

roughly to pressure gradient PG6 is reached. After this, again the structure angle reduces rather rapidly. Thus there appears to be a distinct change in the trend of structure angle as one goes from turbulent to reverse-transitional flow. It is interesting to note that the value of K around which this change of trend is seen to occur is very close to the well-known limiting value of $K = 3 \times 10^{-6}$ that is often quoted in the literature in the context of the onset of relaminarization (see Sreenivasan 1982).

If we take the typical boundary layer thickness δ to be about 15 mm (see table 2), then the streamwise separation between stations L3 and L4 is about 4δ. Even though this distance over which the constancy of structure angle has been observed is not as large as one would want to be able to make any conclusive statements, the possibility of structure angle reaching its asymptotic value in the sink flow configuration appears quite plausible. In view of the short separation between L3 and L4, the last sink flow station L5 (see Dixit & Ramesh 2008) could have been used for the present study, especially to demonstrate the streamwise invariance of structure angle. However the sink flow region ends just after station L5, as seen in Dixit & Ramesh (2008), so that the SHW at L5 and the HW 40 mm downstream of it would detect the structure that is partly inside and mostly outside the sink flow region. This possibility was therefore not pursued.

The expectation regarding the structure inclination angle reaching its asymptotic value in a sink flow may be appreciated by appealing to the following heuristic argument. Figure 12 shows the large-scale structure in a sink flow boundary layer. It will be shown later in § 7 that the local convection velocity $U_c(x, y)$ of the structure in the present study is fairly close to the local mean velocity $U(x, y)$. Thus figure 12 shows point $\boldsymbol{A}$ belonging to the structure with coordinates (x, y) where the convection velocity of point $\boldsymbol{A}$ is $U_c = U(x, y)$. It may be easily shown from the geometry of sink flow (see also Dixit & Ramesh 2008) that each radial mean streamline represents a line of constant $\eta = y/\delta$, with the obvious limiting cases being $\eta = 0$ at the wall and $\eta = 1$ at the boundary layer mean edge. Furthermore since the flow is steady in the mean, the mean pathlines are the same as the mean streamlines. This implies that as the flow proceeds downstream, point $\boldsymbol{A}$ moves (in the mean) to a different x but remains at the same η. Further since the Reynolds number $R_\tau = \delta U_\tau/\nu = \delta_+$ is constant for a given sink flow, it is clear that on each mean streamline, $y_+ = yU_\tau/\nu = (y/\delta)(\delta U_\tau/\nu)$ is also a constant. Thus we have a situation in which point $\boldsymbol{A}$, along with the infinitesimal length of structure around it, moves in x with y_+ (or η) held fixed. Thus if we show that the slope $\mathrm{d}y/\mathrm{d}x$ of this infinitesimal length is independent of x, at a given value of y_+ (or η), then it would amount to the statement that the local structure inclination angle does not change in the streamwise direction.

Assuming that the velocity field $U(x, y)$ is continuous, slope $\mathrm{d}y/\mathrm{d}x$ of the infinitesimal length of structure around point $\boldsymbol{A}$ may be written, at a fixed value of y_+, as

$$\left.\frac{\mathrm{d}y}{\mathrm{d}x}\right|_{y_+} \sim \left.\frac{\partial U/\partial x}{\partial U/\partial y}\right|_{y_+}. \tag{4.3}$$

A similar expression for the orientation of vortex elements has been used by Head (1976) for an APG equilibrium turbulent boundary layer flow. Since the mean velocity profiles at different streamwise stations for a sink flow collapse in all scalings (see Dixit & Ramesh 2008), we can write the mean velocity in the inner scaling as $U_+ = f(y_+)$, where $U_+ = U/U_\tau$ is independent of x and is a function of y_+ alone. Interestingly, in view of figure 8 and table 2, all the considerations in the following that apply to the turbulent sink flow cases (PG1–PG6) apply equally well to the reverse-transitional cases (PG7 and PG8). Substituting the inner scaling $U_+ = f(y_+)$ into (4.3) with simple rearrangements yields

$$\left.\frac{\mathrm{d}y}{\mathrm{d}x}\right|_{y_+} \sim \left(-\Delta_p \frac{C_f}{2}\right)\left[\frac{\mathrm{d}\left(y_+ f\right)/\mathrm{d}y_+}{\mathrm{d}f/\mathrm{d}y_+}\right]_{y_+}. \tag{4.4}$$

As already mentioned, the pressure gradient parameter Δ_p and the skin friction coefficient C_f are constant for a given sink flow; while obtaining (4.4), the constancy condition for C_f has been used. Therefore (4.4) implies that the slope $\mathrm{d}y/\mathrm{d}x$ of the structure at a fixed value of y_+ is independent of the streamwise coordinate x, since all the other quantities on the right-hand side of (4.4) are functions of y_+ alone. This demonstrates that the local structure inclination angle (given by the inverse tangent of the slope $\mathrm{d}y/\mathrm{d}x$) for a fixed value of y_+ (or η) remains invariant in the streamwise direction. Since (4.4) is derived for an arbitrary value of y_+, the result is valid for all values of y_+. This implies that all local inclination angles of the structure are preserved as the structure travels downstream. Thus it is clear that the average inclination angle of the structure would also be preserved. This heuristically explains the expectation regarding the inclination angle of the large-scale structure reaching its asymptotic value in the sink flow.

4.4. *Spatial extent of the large-scale structure*

It is instructive to examine the effect of pressure gradient on spatial extent of the structure in both the streamwise and wall-normal directions. In order to study this aspect, we consider in this section (i) the contours of the cross-correlation coefficient $R_{\tau u}(\Delta x, y)$ and (ii) the estimates of the integral length scale L_{uu}.

Figures 13 and 14 show the contours of $R_{\tau u}(\Delta x, y)$ for all the eight pressure gradients with the SHW at station L4. These have been obtained by projecting the HW signal upstream as well as downstream of the HW by using positive and negative time delays respectively on the HW signal. Boundary layer thickness at M4 (i.e. where the HW probe is located) is used for non-dimensionalization of the axes. There are many interesting features of these contour plots that deserve special mention.

First, one may observe that for a fixed value of $\Delta x/\delta$, larger values of $R_{\tau u}(\Delta x, y)$ occur close to the wall, and they generally decrease in the wall-normal direction as one moves away from the wall. It is also clear that as the magnitude of the FPG increases, regions of highly correlated activity get progressively concentrated close to the wall and also extend downstream. This implies that the structure gets flatter and longer because of increase in the strength of the FPG. Observation of the contours of $R_{\tau u}(\Delta x, y) = 0.2$ (say) clearly reveals this marked increase in the

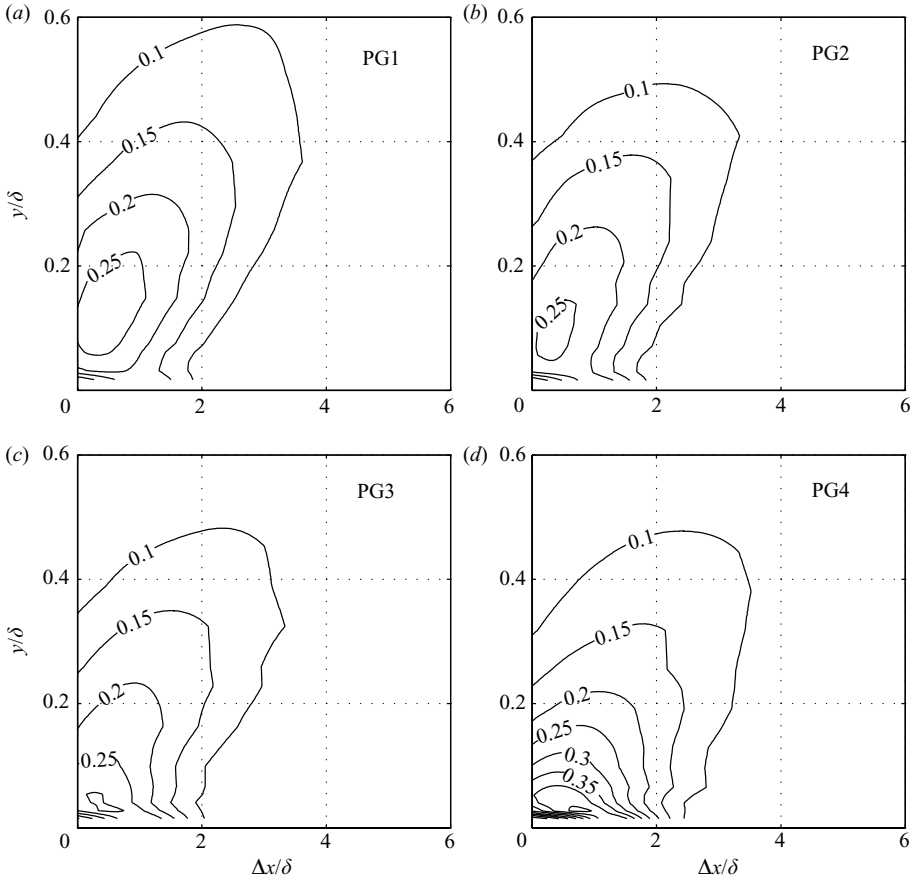

FIGURE 13. Contours of $R_{\tau u}(\Delta x, y)$ for pressure gradients PG1 to PG4. The SHW is at L4 (at the origin of each plot). Boundary layer thickness δ at M4 is used for non-dimensionalization.

streamwise extent of the structure. It is apparent that the contours, of $R_{\tau u}(\Delta x, y) = 0.1$, are somewhat jagged, but this should not be taken to be inadequate convergence of the correlation. This appears to be simply due to weakened correlation between the wall-shear stress and the streamwise velocity fluctuation which involves relatively larger uncertainties even though sufficient boundary layer turnover times are accounted for in the averaging process.

Next, it may be noted that wall-normal extent of the structure that can be identified without ambiguity remains almost the same with variations in the pressure gradient. This may become clear if one observes that the upper portion of the $R_{\tau u}(\Delta x, y) = 0.1$ contour always resides at $y/\delta \approx 0.5$ from the wall.

Another interesting observation is concerned with the magnitude and location of the maximum value of $R_{\tau u}(\Delta x, y)$. Since $R_{\tau u}(\Delta x, y)$ is defined between the wall-shear stress fluctuation and the streamwise velocity fluctuation, one would expect the maximum value of $R_{\tau u}(\Delta x, y)$ to occur at the SHW location, i.e. at the origin of each plot. In other words, the 'eye' of the contour plot should be centred on the SHW location. This expectation comes from what happens in two-point correlations of the streamwise velocity fluctuation measured by two spatially separated HW probes (see for example Krogstad & Skåre 1995). However figures 13 and 14 indicate that

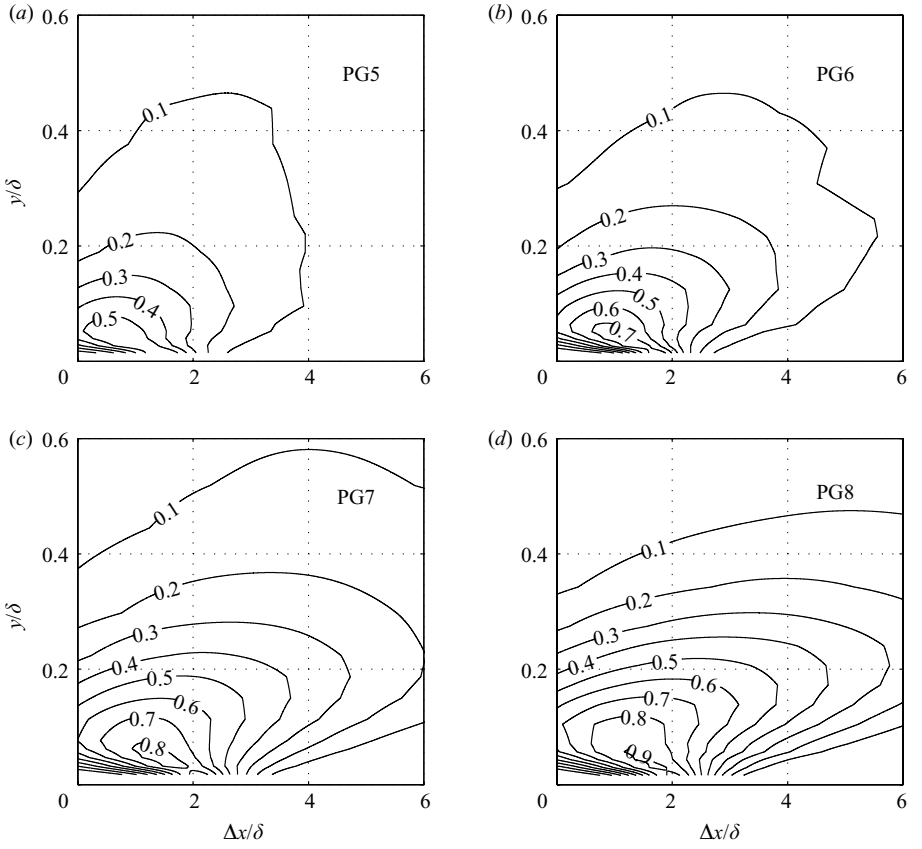

FIGURE 14. Contours of $R_{\tau u}(\Delta x, y)$ for pressure gradients PG5 to PG8. The SHW is at L4 (at the origin of each plot). Boundary layer thickness δ at M4 is used for non-dimensionalization.

this does not happen in the present cases. The eye of the contour plot is seen to be located away from the SHW location (above and downstream of it). Furthermore there appears to be a systematic movement of this eye (towards the wall and further downstream) as the FPG is made progressively severe. In addition there is a clear increase, with the FPG, in the maximum value of $R_{\tau u}(\Delta x, y)$ that occurs at the centre of the eye.

It should be emphasized that this behaviour has been noted previously in the literature by Wark & Nagib (1991) who have employed an array of shear stress sensors and a cross-wire probe for structural and other investigations of a ZPG turbulent boundary layer flow. They have not plotted the contours of $R_{\tau u}(\Delta x, y)$ as has been done here, and therefore the above-mentioned behaviour goes somewhat unnoticed in their paper. Figure 3(*a*) from Wark & Nagib (1991) shows the temporal counterpart of $R_{\tau u}(\Delta x, y)$ (i.e. without making use of Taylor's hypothesis) plotted against the time shift given to the $u(t)$ signal. The cross-wire probe is located directly above the shear stress sensor for this plot. It is seen that as one moves away from the wall, the peak in the correlation occurs at progressively negative time shifts, which is as expected for a structure that is leaning forward in the direction of the flow. However it is clearly seen that the magnitude of peak correlation first increases and then decreases as one moves away from the wall. This implies that the contour plot

in that case would also show the peak correlation occurring above and downstream of the shear stress sensor as in the present cases.

It is clear that 'at the wall', since the streamwise velocity fluctuation is zero its correlation with the wall-shear stress fluctuation has to be zero, as they are not in phase with each other. It is hence conceivable that non-zero values of this correlation should occur away from the wall. While this explains peaking of the correlation away from the wall, it still does not explain why it peaks downstream of the SHW. The use of Taylor's hypothesis does not appear to be the reason for this intriguing behaviour, since exactly the same observation has been made by Wark & Nagib (1991) without using Taylor's hypothesis. Perhaps the key lies in the fact that the correlation under consideration is between wall-shear stress fluctuation and streamwise velocity fluctuation and not between the two streamwise velocity fluctuations recorded by different HW probes.

In the context of increase in the streamwise extent of structure with the FPG (figures 13 and 14), it is instructive to appeal to the experimental results by Krogstad & Skåre (1995) for an APG near-equilibrium turbulent boundary layer close to separation. They have noted that the streamwise spatial extent of the large-scale structure in the case of APG flow is smaller than that in the case of a ZPG flow as may be seen from figures 5(a, b) and 7(a) in their paper. This trend in APG flow is exactly opposite to the one observed here for the FPG flow. This implies that the presently observed trend of increase in streamwise spatial extent of the structure with increase in the FPG is consistent with the results of Krogstad & Skåre (1995) if the sign of pressure gradient is taken into account.

As to the estimates of the integral length scale, the autocorrelation coefficient for stationary streamwise velocity fluctuation $u(t)$ is given by

$$R_{uu}(x, y, \Delta t) = \frac{\overline{u(x, y, t)u(x, y, t + \Delta t)}}{\overline{u^2}}, \tag{4.5}$$

where Δt is the time delay given to the $u(t)$ signal. Using Taylor's hypothesis, the time delay may be converted to spatial distance. Note that $R_{uu}(x, y, \Delta t = 0) = 1$. Now the integral time scale T_{uu} is defined in the standard fashion (see Tennekes & Lumley 1972) as

$$T_{uu} = \int_0^\infty R_{uu}(x, y, \Delta t)\, \mathrm{d}(\Delta t), \tag{4.6}$$

where the integration, in practice, is usually carried out from zero to that value of Δt at which $R_{uu}(\Delta t)$ first crosses the line $R_{uu}(\Delta t) = 0$ (here onwards the dependence on x and y will be dropped for convenience with the understanding that all these quantities are local). Note that T_{uu} may be interpreted as the area under the $R_{uu}(\Delta t)$ curve being concentrated in a rectangle of width T_{uu} and unit height (i.e. the maximum value for $R_{uu}(\Delta t)$). The integral time scale T_{uu} is related to the integral length scale L_{uu} through Taylor's hypothesis as

$$L_{uu} = -U_c T_{uu}, \tag{4.7}$$

where $U_c = U_c(x, y)$ is the convection velocity taken to be the same as the local mean velocity, i.e. $U_c = U(x, y)$. Note that because of the use of (4.7) L_{uu} has a negative sign, and its magnitude is indicative of the typical spatial extent over which $u(t)$ is correlated with itself.

Figure 15 shows wall-normal distribution of non-dimensional magnitude of the integral length scale (L_{uu}/δ) plotted for all pressure gradients with the HW probe

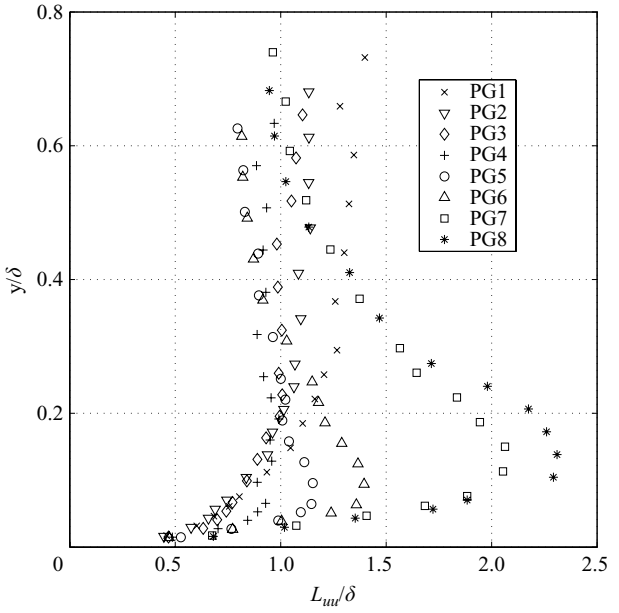

FIGURE 15. Wall-normal distribution of the magnitude of the integral length scale L_{uu} based on the autocorrelation coefficient $R_{uu}(\Delta t)$ for all pressure gradients. The HW is at M4.

at station M4. It is evident from figure 15 that the integral scale, especially in the near-wall and intermediate regions, shows marked increase as the pressure gradient is made more favourable. This reconfirms that the spatial extent of the correlated activity indeed increases with the FPG.

Thus from the discussion on the structure inclination in § 4.3 and the present discussion on the contour plots and the integral length scale, we may now conclude that the structure becomes flatter (the structure angle decreases) and longer (the streamwise spatial extent increases) as the pressure gradient is increased to make it more favourable.

4.5. *Plausible structural models for sink flow turbulent boundary layers*

Hairpin vortices are perhaps the most widely accepted and dominantly occurring structural elements that populate the entire turbulent boundary layer as discussed already in § 1. The shapes of individual hairpins and the inclinations of hairpin packets (formed because of structural self-organization) are possibly two independent issues (see Adrian *et al.* 2000), and in this subsection we try to connect the present experimental results from §§ 4.1–4.4 to these ideas. This connection, by its very nature, is rather speculative, since the present study based on the HW anemometry measurements of two-point correlations is indeed incapable of going as far as for example a PIV or a DNS study in deducing and confirming the above-mentioned structural aspects in detail. Nevertheless attempts to make such connections may take us quite far in terms of shedding useful light on some conceptually important issues such as the mechanism of relaminarization or reverse transition by a strong FPG, as we shall see shortly in the next section. In this subsection, we first propose a plausible shape of the individual hairpin for a sink flow turbulent boundary layer without considering any structural self-organization. This will then be followed by a

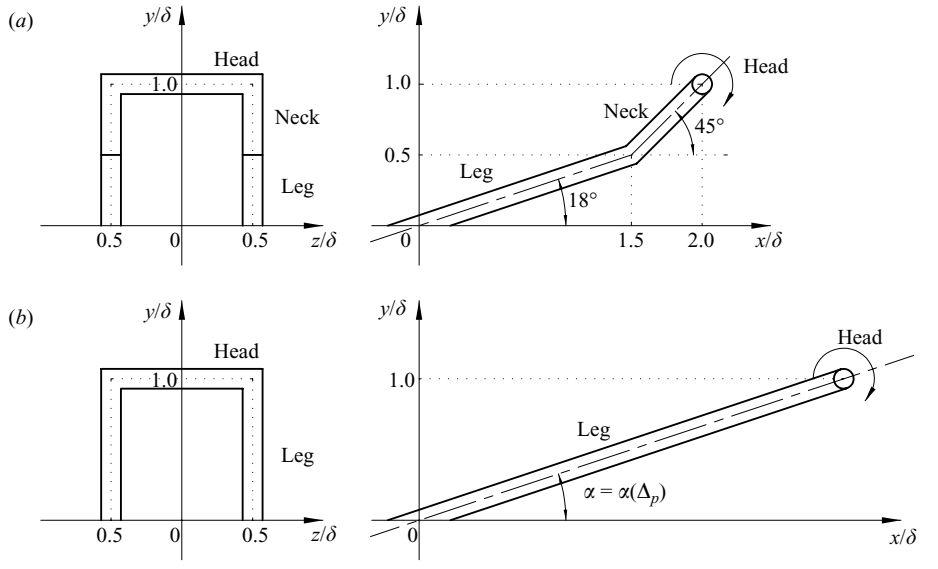

FIGURE 16. (*a*) Typical ZPG eddy (a slanted Π-eddy) proposed by Marusic (2001) and (*b*) the present proposal of a typical sink flow turbulent boundary layer eddy (a shallow Π-eddy). The eddy nomenclature (head, neck and leg) is as given in Robinson (1991).

discussion regarding the hairpin packet inclinations (i.e. with the possible structural self-organization taken into account) in the light of the present experimental results.

The prevalent model for a typical eddy in a ZPG turbulent boundary layer flow is the attached eddy inclined to the wall at about 45°, leaning forward in the downstream direction (see Perry & Chong 1982; Perry *et al.* 1986). As mentioned in § 1, Marusic (2001) has shown that a more appropriate form of the ZPG eddy would be a slanted Π-eddy (see figure 16*a*), since the calculations based on it agree better with the experimental data. Further, there appears to be a close correspondence between (i) the shallow-angled (18°) leg of the eddy and the inner region of the mean velocity profile and (ii) the 45° neck of the eddy and the outer part of the mean velocity profile. In other words, two-tiered structure of the slanted Π-eddy appears to be consistent with the corresponding two-layered structure of the ZPG turbulent boundary layer.

Now in the case of a sink flow turbulent boundary layer, it is well known that there is complete overlap of the inner and outer layers (Coles 1957; Jones *et al.* 2001; Dixit & Ramesh 2008), and the log law extends almost up to the edge of the boundary layer, i.e. a pure wall-flow. Therefore, based on an analogy to the ZPG scenario, we may speculate that the typical eddy in a sink flow turbulent boundary layer might just be a shallow Π-eddy (see figure 16*b*) made up only of the shallow-angled leg part extending all the way from the wall with the head located near the boundary layer edge (similar to the type A eddy of Perry *et al.* 2002). In absence of any structural self-organization, the structure inclination angle as measured in the present study must correspond to the angle of this leg and would thus be a function of the pressure gradient (see §§ 4.2 and 4.3) as seen in figure 16(*b*). While the proposed shallow Π-eddy is similar to the type A eddy structure proposed by Perry *et al.* (2002), the difference between them appears to be that while the latter yields a pure wall-flow with the universal log law in the inner region (as in ZPG flows) the former is expected to yield a family of pure wall-flows with the non-universal log laws depending on the strength of the pressure gradient.

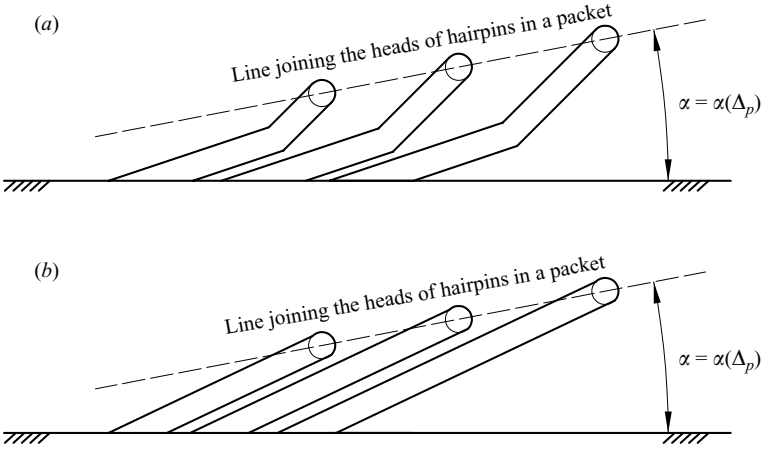

FIGURE 17. Possible spatially coherent hairpin packets in sink flow boundary layers and their pressure-gradient-dependent inclinations. (*a*) Packet of slanted Π-eddies similar to those in ZPG turbulent boundary layer flows and (*b*) packet of shallow Π-eddies as per the present proposal in figure 16(*b*).

Next we consider structural self-organization. Following the ZPG case, we would like to explore the possibility that the structure inclinations measured in the present study using two-point correlations correspond to the 'packet inclinations' (see Adrian *et al.* 2000; Christensen & Adrian 2001; Lee & Sung, 2009) rather than the inclinations of individual hairpins. In that case, whatever may be the shape of the individual hairpins, the inclination of the ramp-like line connecting the heads of hairpins in a packet must be a function of the pressure gradient. This situation is shown schematically in figure 17(*a*, *b*).

Whether such structural self-organization may be expected in sink flow situations is unclear at present. In view of relatively low Reynolds numbers in the present study, it may be appropriate to relate the 'backs' of outer layer bulges to the outlines of the hairpin packets in a fashion similar to the low-Reynolds-number ZPG turbulent boundary layer flows (see Adrian *et al.* 2000). However the fact that the mean entrainment is zero in sink flow boundary layers (i.e. all the Reynolds numbers are streamwise constant for a given sink flow) may well be related to the altered structure of the outer layer bulges in comparison with the ZPG case. More importantly, if one views the streamwise coherence associated with a hairpin packet as a means of bringing in the 'non-local' influences, then the hairpin packet scenario goes against the 'perfect equilibrium' (perfectly 'local' scaling) character exhibited by sink flow boundary layers. On the other hand, the contours of $R_{\tau u}(\Delta x, y)$ (figures 13 and 14) and the estimates of the integral length scale (figure 15) indicate the present of strong streamwise coherence that may perhaps be taken as a support for the hairpin packet paradigm. Such a strong streamwise coherence may, however, be simply due to the increased streamwise dilatation of the individual hairpin eddies due to the FPG (that is not a factor in the ZPG case). As mentioned before in § 1, the recent DNS study of equilibrium APG turbulent boundary layers by Lee & Sung (2009) shows apparent increase in the streamwise separation between the hairpin heads in a packet for APG flow as compared with the ZPG flow. Extending this to the strong-FPG case, one may expect more closely spaced hairpins (than the ZPG) in a packet (if the packet itself exists) or even merging of these closely spaced hairpins into a single strong

hairpin. This would be indicative of the nature of the flow becoming more 'local'. DNSs and careful PIV measurements with sink flow boundary layers at different pressure gradients and Reynolds numbers would certainly shed important light on these presently speculative issues of structures and their organization.

5. Structural model of relaminarization of turbulent boundary layers in strong FPGs

The phenomenon of relaminarization or reverse transition of turbulent boundary layers when subjected to strong streamwise FPGs may be explained in the light of large-scale structural aspects and their behaviour in strong FPGs. When an initially turbulent boundary layer is subjected to a sufficiently strong streamwise FPG, the mean flow development is chiefly governed by pressure and viscous forces with turbulent transport of streamwise mean momentum becoming comparatively negligible. Thus as far as the mean flow is concerned, such a flow is like a pressure-gradient-driven laminar boundary layer flow. This phenomenon is called relaminarization or reverse transition by a strong FPG. If the FPG is strong but not enough to fully relaminarize the flow, then the state of the flow may be somewhere in between the fully turbulent and fully relaminarized state. This may be called the reverse-transitional turbulent boundary layer flow. Flows PG7 and PG8 in the present study appear to be reverse-transitional flows, since the mean velocity profiles in these flows are less full compared with the fully turbulent cases (PG1 for example) and more full compared with the laminar sink flow solution (see figure 2). In view of the experimental results obtained so far in the present study, the model proposed by Narasimha & Sreenivasan (1973) for the quasi-laminar limit of reverse transition (in this connection, see also Narasimha & Sreenivasan 1979; Sreenivasan 1982) and the plausible structural models discussed in § 4.5, we may now attempt to develop a structural explanation of the process of reverse transition in sink flow turbulent boundary layers. First, we shall briefly discuss the essence of the quasi-laminar limit of the reverse-transition process by a strong FPG as proposed by Narasimha & Sreenivasan (1973). Next, we shall show how the structural models discussed in § 4.5 may be used to explain the reverse-transition process in sink flow turbulent boundary layers.

Narasimha & Sreenivasan (1973) have shown that in the final stages of reverse transition by a strong FPG, the boundary layer flow field may be divided into two parts: (i) the outer part of the boundary layer that behaves as a rotational, inviscid flow describable by the Euler equation and (ii) the inner viscous part of the boundary layer that is governed in the mean essentially by the laminar flow equations (i.e. without any modelling for turbulence). They have argued that the turbulent stresses themselves 'do not' vanish; i.e. the turbulence is 'not' killed off completely; the turbulent stresses are nearly frozen in magnitude as the boundary layer passes through various stages of relaminarization. It is the turbulent transport $\partial(-\overline{uv})/\partial y$ of the mean streamwise momentum that is rendered negligible by the dominating pressure forces. This is the so-called quasi-laminar limit. Note that since turbulence is not destroyed in such cases, this type of relaminarization is referred to as 'soft' relaminarization (Narasimha 1983). We can reconcile this picture with the eddy structural viewpoint (i.e. both individual hairpins and hairpin packets) as discussed below.

First of all, it is important to note that the turbulent transport term in the mean streamwise momentum equation may be written (see Tennekes & Lumley 1972), in

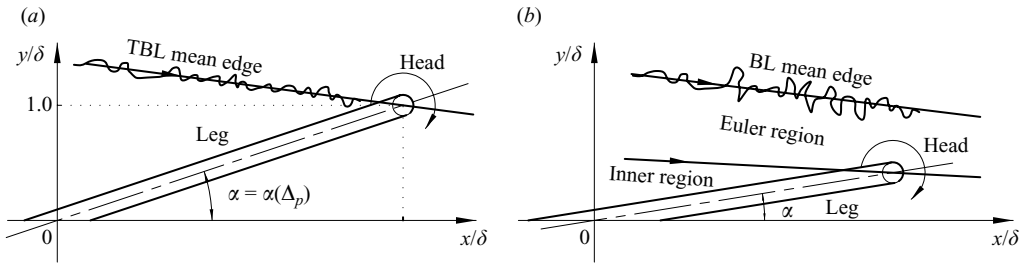

FIGURE 18. Schematic of typical eddies in (*a*) a sink flow turbulent boundary layer and (*b*) a sink flow reverse-transitional boundary layer.

the present notation, as

$$\frac{\partial\,(-\overline{uv})}{\partial y} = \overline{v\omega_z} - \overline{w\omega_y}, \tag{5.1}$$

where ω_y and ω_z are the vorticity fluctuations in the wall-normal and spanwise directions respectively and u, v and w are the velocity fluctuations in the streamwise, wall-normal and spanwise directions respectively. It must be noted that the prerequisite condition for validity of (5.1) is $\partial\overline{u^2}/\partial x \ll \partial(-\overline{uv})/\partial y$ which is indeed fulfilled by the boundary layers in the present study (see Dixit & Ramesh 2008).

From the viewpoint of individual hairpins without any self-organization and the proposed pressure gradient dependence of their inclination (see § 4.5 and figure 16), we may explain the sink flow reverse-transition process as follows. If we treat the structure in a sink flow turbulent boundary layer as a vortex of the shape similar to that shown in figure 16(*b*), we observe that the vorticity from the leg is largely orientated in the streamwise direction (i.e. $\omega_x \gg \omega_y$) as a consequence of the shallow inclination of the leg (quasi-streamwise vortices according to Robinson 1991). Therefore we have a case in which the leg contributes little to the gradient $\partial\,(-\overline{uv})\,/\partial y$ of Reynolds shear stress; i.e. the second term in (5.1) is negligible. This implies that the major contribution towards $\partial\,(-\overline{uv})\,/\partial y$ comes from the 'head' of the eddy where the dominant component of fluctuating vorticity is ω_z. This suggests that the turbulent transport due to $\partial\,(-\overline{uv})\,/\partial y$ is likely to be large in the outer part of the sink flow turbulent boundary layer, since the head of the eddy resides close to the mean edge of the turbulent boundary layer (see figure 18*a*).

If the FPG is now made sufficiently large for the onset of relaminarization, we may conceive of a situation in which the eddy inclination has reduced because of the increase in the FPG (consistent with figure 10) and the head of the eddy has moved away from the mean edge inside the boundary layer. This situation is shown schematically in figure 18(*b*). In view of (5.1) and the discussion in the previous paragraph, the movement of eddy head away from the mean edge towards inner region of the boundary layer would cause turbulent transport to become negligible in the outer part of the layer close to the mean edge. Furthermore, because of the weak gradient of mean velocity in the region close to the mean edge, the viscous transport there can also be expected to be negligible. Consequently, the outer region starts behaving like an inviscid layer which is nonetheless rotational because of all the vorticity that has been acquired upstream. This region is hence describable by the Euler equation (see figure 18*b*) as in the model of Narasimha & Sreenivasan (1973).

It is known (see Rotta 1962) that the wall-normal velocity fluctuation v decreases at a faster rate, compared with the other two components u and w, as the wall is approached (the so-called blocking effect of the wall). Thus the contribution towards

$\partial(-\overline{uv})/\partial y$ coming from the head of the eddy in the inner region is also expected to reduce, not so much because of the reduction in ω_z but apparently because of the reduction in magnitude of v (see 5.1). This implies that turbulent transport in the inner region may also be expected to be small especially in comparison with the viscous transport which is expected to be large because of large gradients of the mean velocity in the near-wall region. Thus in the limiting case in which the FPG becomes so large that the quasi-laminar limit is reached, we may expect the inner region to be governed mainly by pressure and viscous forces with the turbulent transport becoming comparatively negligible.

It has been mentioned in § 4.2 that the correlation between the fluctuating wall-shear stress and the streamwise velocity fluctuation becomes weak at large wall-normal distances. Now this might be due to (*a*) the presence of a structure with a region of weak correlation that is difficult to detect or (*b*) the absence of any structure altogether. By perusal of figures 13(*a*) and 14(*d*), we associate the former possibility with the turbulent case and speculate that the latter might be associated with the reverse-transitional case. Table 2 shows that the boundary layer thicknesses in these cases are not very different. This lends credence to the speculation that the loss of correlation in PG8 case may indeed be genuinely associated with the propensity of the outer region to become rotational and inviscid.

Next, from the viewpoint of hairpin packets and the proposed pressure gradient dependence of their inclinations, i.e. the packet inclinations (see § 4.5 and figure 17), we may explain the sink flow reverse-transition process in a much similar fashion as for the individual hairpins. In the case of packets, inclination of the line connecting the heads of hairpins in a packet is a function of the pressure gradient as discussed in § 4.5. It is thus evident that when this inclination reduces with the increase in the FPG, the 'heads' of hairpins in the packet would come close to the wall; i.e. the outer region of the turbulent boundary layer would become increasingly free of the turbulent transport effected by the heads. Therefore the explanations given in the preceding paragraphs for the individual hairpins also apply to the hairpin packets.

Thus the phenomenon of relaminarization by a strong FPG may be explained in terms of the experimentally observed behaviour of the large-scale organized structures. It must be noted that the above-given explanations are fairly general and may apply even to a non-sink flow situation in which the flow may not be in equilibrium. In that case, the response of the structure to the FPG (which might be changing rapidly in the streamwise direction) is of course not expected to be local. However the process of relaminarization may still be related to the structure inclination in much the same way as demonstrated here for the sink flow cases.

Notice that the very presence of large-scale structure implies presence of $(-\overline{uv})$, but it is the gradient $\partial(-\overline{uv})/\partial y$ which reduces as the structure tilts more towards the wall. This means that the turbulence does not die off completely, but the transport of streamwise mean momentum, effected by it, becomes comparatively negligible in a strong FPG, and this is the essence of the so-called soft relaminarization (Narasimha 1983) as discussed before in this section. In this way, a deeper appreciation of the phenomenon of soft-relaminarization may be gained by invoking such structure-based arguments.

6. Experimental validation of Taylor's hypothesis for the present study

Taylor's hypothesis has been used in the present study to obtain the cross-correlation coefficient $R_{\tau u}(\Delta x, y)$ from the measured time-series data as explained previously in § 2. This section deals with the validity of Taylor's hypothesis that has been established

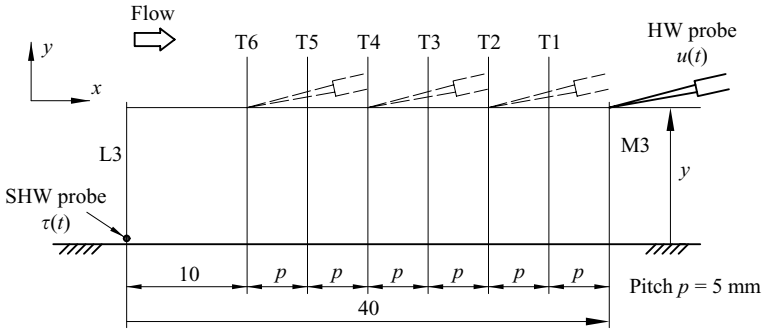

FIGURE 19. Probe arrangement used for validating Taylor's hypothesis. The SHW is at L3. Only 1 of the 11 y locations is shown for clarity. The dotted HW probes indicate physical movement of the HW to the grid points. All dimensions are in millimetres. The figure is not to scale.

experimentally for the present study by making use of local mean velocity as the convection velocity. A brief account of the related literature will be given in the next section.

Since the present study is concerned with boundary layers, turbulent and reverse transitional in moderate and strong FPGs, it was considered important to validate Taylor's hypothesis experimentally without relying on the results that have so far been obtained primarily in the ZPG situations (see § 7).

Figure 19 shows the experimental arrangement adopted for this exercise. The SHW probe was at L3. Six streamwise locations T1–T6 were chosen as indicated in figure 19. Eleven wall-normal locations in the range of 1–8 mm from the wall were selected. The choice of wall-normal locations was guided by the typical extent of the linear region of the large-scale structure as seen in figure 10. The HW probe was traversed in the wall-normal direction at each streamwise station (T1–T6) through the same 11 wall-normal locations. Thus a grid of 66 measurement locations was formed (6 streamwise locations and 11 wall-normal locations at each streamwise location). The HW probes shown using the dotted lines in figure 19 indicate that the HW probe, originally located at M3, was moved physically and taken to each of the above-mentioned grid points. It was ensured that the wall-normal locations selected for this validation exercise were the same as those in the basic HW probe traverse at M3 carried out for the original structure angle measurements.

Signals from the SHW (at L3) and the HW (at all the grid points) were acquired with appropriate sampling rates and durations (see table 1), without any initial time delay, for four representative pressure gradients PG1, PG3, PG6 and PG8 covering the entire range. These signals were directly correlated, with zero time delay ($\Delta t = 0$), to get the 'direct' measurement of cross-correlation coefficient $R_{\tau u}(\Delta x, y)$ at all the grid points. Next, from the original HW data at M3 (and the corresponding SHW data at L3) taken during the structure angle investigations, the time delay Δt given to the HW signal was appropriately adjusted so as to extract the 'Taylor's estimate' of the cross-correlation coefficient $R_{\tau u}(\Delta x, y)$ at all the grid points. If the direct values of cross-correlation coefficient $R_{\tau u}(\Delta x, y)$ agree well with the corresponding Taylor's estimates (within the typical measurement uncertainty), then it may be concluded that Taylor's hypothesis is valid.

Note that this exercise used only positive time delays given to the HW signal; i.e. HW signals were projected only upstream of the HW. This however is not of much

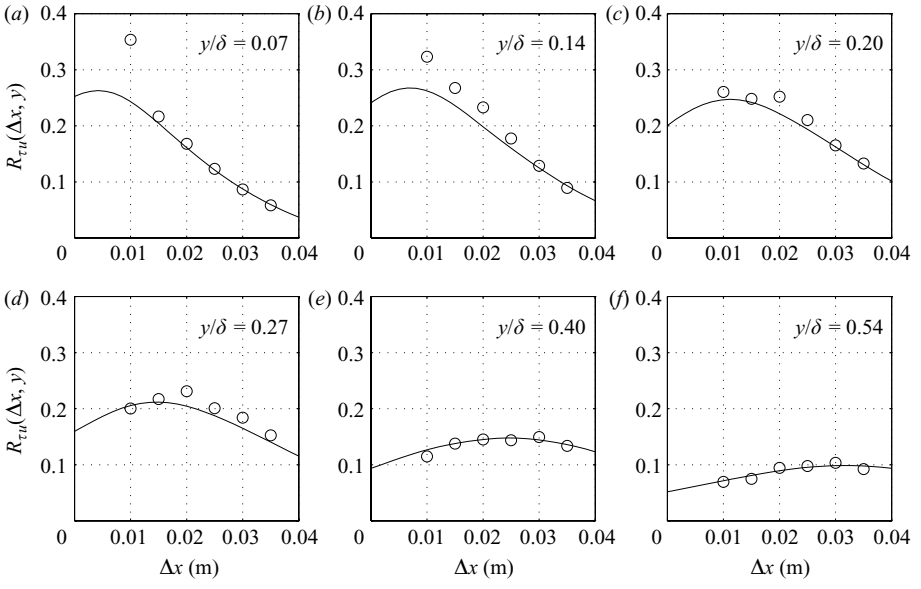

FIGURE 20. The cross-correlation coefficient $R_{\tau u}(\Delta x, y)$ at six representative wall-normal locations for pressure gradient PG1. The solid line indicates Taylor's estimate, while the circles indicate the direct measurement with zero time delay. The SHW is at L3 ($\Delta x = 0$), and the HW is at M3 ($\Delta x = 0.04$ m).

concern, since the peak value of $R_{\tau u}(\Delta x, y)$ was seen to occur mostly upstream of the HW in all the flows studied (see figure 10). However for the contour plots of figures 13 and 14, both types of delays were used, and therefore those plots assume the validity of Taylor's hypothesis in the downstream direction as well. Even though this aspect is not demonstrated here in the present exercise, it is not unreasonable to expect that Taylor's hypothesis would be equally valid both upstream and downstream of the HW especially when the maximum projection distances in both the directions are of the same order (40 mm upstream and 60 mm downstream).

Figure 20 shows the comparison of Taylor's estimate and the direct measurement of the cross-correlation coefficient $R_{\tau u}(\Delta x, y)$ for the weakest pressure gradient PG1 at six representative wall-normal locations. Except for the first two wall-normal locations at station T6 ($\Delta x = 0.01$ m), overall agreement between the two methods, within the experimental uncertainty, is quite reasonable, giving an indication of the validity of Taylor's hypothesis (with local mean velocity as the convection velocity). Note that the apparent scatter in the present results (figures 20 and 21) should be compared with the typical scatter in similar studies reported in the literature (see for example Uddin, Perry & Marusic 1997). Such a comparison shows that the present scatter is indeed very much typical of such studies and is therefore insignificant.

Figure 21 gives a similar comparison of Taylor's estimate and the direct measurement of $R_{\tau u}(\Delta x, y)$ for the strongest pressure gradient PG8. Again here, within the experimental uncertainty, the agreement between the two methods is quite reasonable, suggesting that even in such a strong-pressure-gradient situation, Taylor's hypothesis (with local mean velocity as the convection velocity) works fairly well over the range of projection distances Δx_p (0–40 mm) used in this exercise. As mentioned before, Taylor's hypothesis is expected to work well even for downstream projections though not demonstrated here.

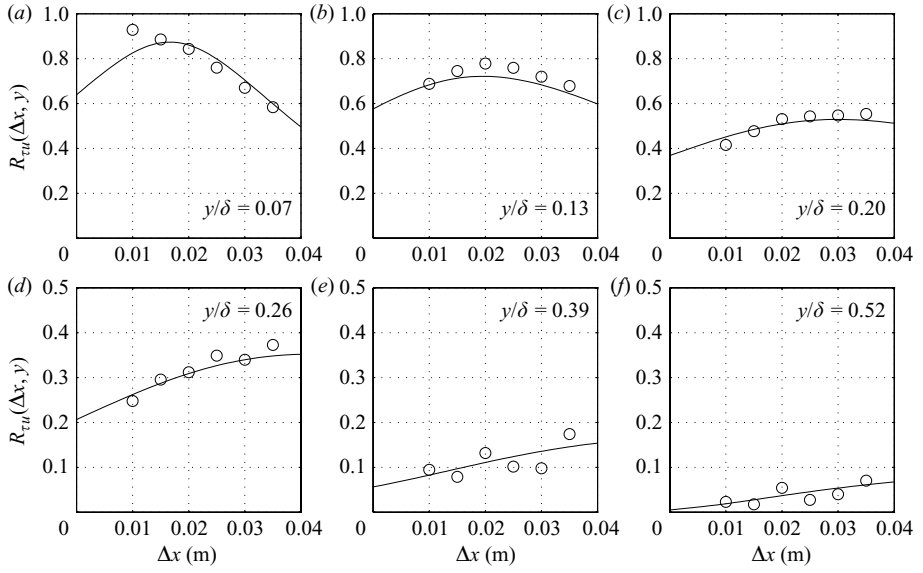

FIGURE 21. Cross-correlation coefficient $R_{\tau u}(\Delta x, y)$ at six representative wall-normal locations for pressure gradient PG8. The solid line indicates Taylor's estimate, while the circles indicate the direct measurement with zero time delay. The SHW is at L3 ($\Delta x = 0$), and the HW is at M3 ($\Delta x = 0.04$ m). Note the change of scale for the ordinate.

The apparent disagreement between Taylor's estimate and the direct measurement at the first two wall-normal locations at station T6 ($\Delta x = 0.01$ m), as seen in figures 20(*a*, *b*) and 21(*a*), deserves some discussion. The first reason one might suspect for such disagreement is the possible contamination of flow caused by the presence of the SHW. This contaminated flow would be seen by the HW especially when it is close to the wall. If one considers the SHW sensor as a small step in the flow (of height $h = 60\,\mu$m approximately), then the flow over it may be described as having 'two weak perturbations' according to Bradshaw & Wong (1972), one before and one after the step. These perturbations are 'weak' because the ratio of step height h to local boundary layer thickness δ is approximately 0.004 which is far less than unity. For 'strong' perturbations $h/\delta = O(1)$, and these situations are studied notably by Bradshaw & Wong (1972) (experiments and calculations) and Le, Moin & Kim (1997) (DNS). These studies have concluded that the relaxation of flow to the normal boundary layer downstream of the step is a very slow process and typically takes more than 50 step heights when $h/\delta = O(1)$. Such a slow relaxation may be attributed to the fact that these 'strong' perturbations essentially alter the outer layer structure which is known to have long memory (see Clauser 1956) in comparison with the inner layer which recovers relatively quickly, possibly because of the influence of the wall. In the present cases, since the ratio $h/\delta \ll 1$, only the part of inner layer very close to the wall is going to be perturbed because of the presence of the SHW. In view of the above-given discussion, this effect is expected to dissipate quickly downstream and not extend to distances as large as, say, $50h$. Thus the disturbance caused by the SHW affecting either Taylor's estimate or the direct measurement appears to be unlikely in the present study.

The second and the likely reason however appears to be the uncertainty in the measured wall-normal distance at station T6. For stations T1–T5, the distance of the

HW sensor from the wall was measured by setting the zero reading for the wall-normal distance using the electrical continuity method. This method involved establishment of electrical continuity between the electrically conducting test plate and the HW sensor by physically taking the HW probe down towards the plate and touching it very carefully. This exercise was carried out at the free-stream velocity of measurement so as to account for the true wall-normal distance that depends on the deflection of the HW probe holder because of the loading caused by the flow. For station T6 however, it was not possible to implement this method because of the presence of electrically non-conducting Teflon plug that was carrying SHW L3. Station T6 was located on the surface of this Teflon plug, and therefore the zero reading for wall-normal distance of the HW sensor was decided essentially by eyeballing. The uncertainty in the wall-normal distance, at T6, is therefore expected to be larger than that at the remaining stations, and its effect is expected to be severe for the wall-normal locations close to the plate. As one moves away from the wall further into the boundary layer, one would expect this effect to reduce. This uncertainty in the wall-normal distance would increase the uncertainty in the directly measured values of $R_{\tau u}(\Delta x, y)$ at T6, especially because correlations do reach large values close to the wall, and the reduction in correlation is relatively more rapid near the wall as compared with distances farther away from the wall. This therefore appears to be the most probable reason for the apparent disagreement seen at station T6 in figures 20 and 21. It is worth noting that the behaviour of the eye of contour plots in the present study and the inferred behaviour of the same from the data of Wark & Nagib (1991) are remarkably similar, even though the former makes explicit use of Taylor's hypothesis, whereas the latter does not (see § 4.4 and figures 13 and 14). This implies that the use of Taylor's hypothesis in the present study is quite reasonable. It is to be noted that other studies especially in atmospheric flows, where measurements have been made very close to the wall, have successfully applied Taylor's hypothesis (Marusic & Heuer 2007) to estimate the structure inclination. This strengthens our view of the uncertainty in the measured wall-normal distance at station T6 (and hence in the direct measurement of $R_{\tau u}(\Delta x, y)$) being the most probable reason for the apparent disagreement between Taylor's estimate of $R_{\tau u}(\Delta x, y)$ and the corresponding direct measurement at station T6.

Figure 22 shows, in a compact manner, the direct value of the cross-correlation coefficient $R_{\tau u}(\Delta x, y)$ plotted against the corresponding Taylor's estimate for the entire validation exercise. All the 6 streamwise stations (T1–T6), all the 11 wall-normal locations (from 1 to 8 mm) and all the 4 pressure gradients (PG1, PG3, PG6 and PG8) are covered in this figure. Clustering of all the data points around the 45° line (which indicates equality between the ordinate and the abscissa) confirms that Taylor's hypothesis (with local mean velocity as the convection velocity) works fairly well for all the flows in the present study.

Before ending this section, few remarks on the possible conditions that are required to be satisfied for the safe use of Taylor's hypothesis in pressure-gradient-driven boundary layer flows are in order. The presence of the streamwise pressure gradient introduces a streamwise length scale $L' = U_\infty/(\mathrm{d}U_\infty/\mathrm{d}x)$ (see also Dixit & Ramesh 2008). One chief requirement therefore appears to be that the projection distance Δx_p (see figure 1*b*) must be much smaller in comparison with L', i.e. $\Delta x_p/L' \ll 1$. In the present study, the maximum value of Δx_p is 60 mm (with the negative time shift), while L' is typically of the order of a metre or so. Thus in the present study, Δx_p is only about 6 % of L', a possible reason for the observed validity of Taylor's hypothesis. Another related aspect is that while using Taylor's hypothesis, we use the

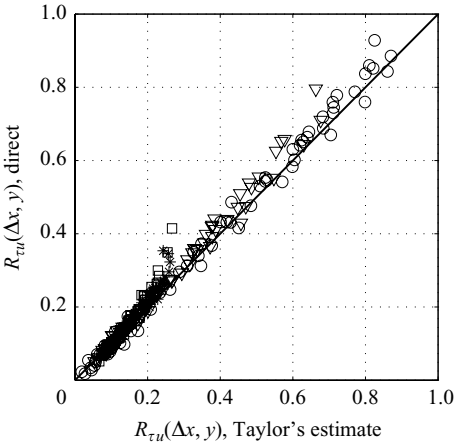

FIGURE 22. The direct value of the cross-correlation coefficient $R_{\tau u}(\Delta x, y)$ plotted against the corresponding Taylor's estimate for all the data in the validation exercise. The 45° solid line indicates equality between the ordinate and the abscissa.

local mean velocity at the HW location as the 'constant' convection velocity. However over the projection distance Δx_p, the local mean velocity and hence the convection velocity are not strictly constant because of the presence of the pressure gradient. Thus the use of Taylor's hypothesis with constant convection velocity would be permissible only if the fractional change in local mean velocity (which may be taken to be of the order of fractional change in U_∞) over the projection distance were small. Note that the condition $\Delta x_p/L' \ll 1$ already takes this aspect into account. Yet another, but again related, consideration could be the inclination of the mean streamlines of the flow. If the streamlines are converging (accelerating flow) or diverging (decelerating flow) rapidly, large projection distances would be inappropriate. In the present case, the angle of a mean streamline at the edge of the boundary layer is typically 1° so that a projection distance of 40 mm amounts to 0.7 mm wall-normal displacement away from the same streamline at the boundary layer edge. Inside the boundary layer this effect would be still less severe.

In view of these considerations, we may justify the streamwise spatial separation of 40 mm between the SHW and HW probes. For all the present flow cases, the large-scale structure detected mostly resides upstream of the HW except for PG6–PG8. Thus for the most part of the present study, only positive time delays are adequate.

7. Convection velocities from space–time correlations

Before proceeding further with the present results, it is instructive to briefly recapitulate the relevant literature on convection velocities and Taylor's hypothesis. For structure angle measurements, Brown & Thomas (1977) have used HW and shear stress sensors for two-point cross-correlations and have found that the structure convection velocity is almost constant with the distance from the wall and is given by $U_c = 0.8U_\infty$ which is consistent with the suggestion of Hussain (1983). The validity of Taylor's hypothesis for inferring structure angles in ZPG turbulent boundary layer flows has been demonstrated by Uddin *et al.* (1997). They have used two HW probes for obtaining two-point correlations and have shown that a convection velocity $U_c = 0.8U_\infty$ is more appropriate to use than the local mean velocity $U(y)$. Krogstad,

Kaspersen & Rimestad (1998) have also used two-point correlations using two HW probes and have found that the 'event' convection velocity is a function of both the distance from the wall and the 'scale' of the detected event (a sweep or an ejection), which is an interesting observation. For the large-scale events they have found that the convection velocity is very close to the local mean velocity. Österlund (1999), by making use of the two-point cross-correlation between the wall-shear stress fluctuation and the streamwise velocity fluctuation, has demonstrated that the convection velocity of the structure is constant close to the wall up to y_+ of about 30, and from there outwards it closely matches with the local mean velocity. Marusic (2001) has used $U_c = 0.8U_\infty$ for inferring structure angles in laboratory ZPG turbulent boundary layers using two HW probes. Marusic & Heuer (2007) have recently shown that the inferred structure angle results strongly depend upon the wall-normal separation between two velocity measuring probes. Instead they have suggested that measurement of structure inclination angle is more robust if a shear stress probe is used in conjunction with a velocity probe to obtain the two-point cross-correlation. They have used $U_c = U(y)$ for inferring structure angles in the laboratory ZPG turbulent boundary layers as well as in the near-neutral atmospheric surface layer on the Utah salt flats. Dennis & Nickels (2008) have demonstrated that Taylor's hypothesis works quite well for the entire turbulence field at least up to projection distances of about 6δ, where δ is the boundary layer thickness. Their measurements have been done using PIV in the logarithmic region of a ZPG turbulent boundary layer. At the wall-normal location of their investigation, they have found that the appropriate convection velocity U_c in the plane of measurement is about 84 % of the free-stream velocity U_∞ and is almost equal to the local mean velocity $U(y)$. From this observation Dennis & Nickels (2008) have noted that the convection velocity corresponds very well with the local mean velocity, at least at the wall-normal location of their investigation. It is to be noted that all the above-mentioned references have made use of the ZPG turbulent boundary layer flow for these investigations.

In this section, we now discuss the appropriate choice of structure convection velocity for the present experiments. The exercise for validating Taylor's hypothesis also allowed estimation of the convection velocities of the large-scale structure. Referring to figure 19, if the HW probe is at a given grid point and the SHW probe is at L3, the exercise of Taylor's hypothesis validation makes use of the 'zero-time-delay' ($\Delta t = 0$) correlation between the two fluctuating signals $\tau(t)$ and $u(t)$ to get the direct value of the cross-correlation coefficient $R_{\tau u}(\Delta x, y)$. Now for the same pair of signals, one may delay the $u(t)$ signal and find out the time delay $\Delta t = \Delta t_{max}$ for which the cross-correlation coefficient reaches its maximum. Furthermore since the HW probe is located at a known grid point, Δx is known. For a given y-level, Δt_{max} is obtained corresponding to each known Δx (total seven stations, M3 and T1–T6), and the plot of Δx versus Δt_{max} is constructed. This plot is typically seen to exhibit a fairly linear behaviour, and the slope of best-fit line (least squares method) gives the local convection velocity $U_c(y)$ at that y-level (see Österlund 1999).

This exercise of obtaining the local convection velocity $U_c(y)$ was carried out for all the four pressure gradients (PG1, PG3, PG6 and PG8) mentioned in the previous section. Figure 23 illustrates the above-mentioned procedure for extreme pressure gradients PG1 and PG8. Since the peak correlation occurs closer to the HW location for stronger pressure gradients, the wall-normal extent available for convection velocity estimation is limited for PG8 as compared with PG1 (see figure 23).

Figure 24(a) shows the local convection velocity $U_c(y)$ compared with the local mean velocity $U(y)$ for four pressure gradients PG1, PG3, PG6 and PG8. It may be

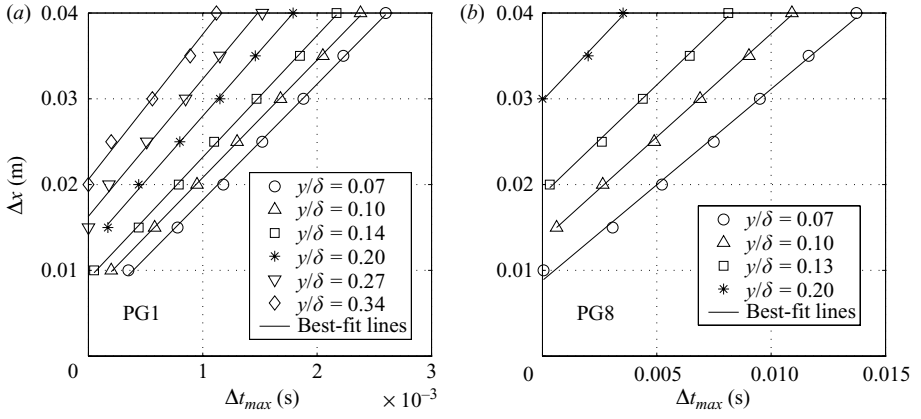

FIGURE 23. Determination of the local convection velocity $U_c(y)$ illustrated for extreme pressure gradient cases: (*a*) PG1 and (*b*) PG8. The slope of a best-fit line gives $U_c(y)$.

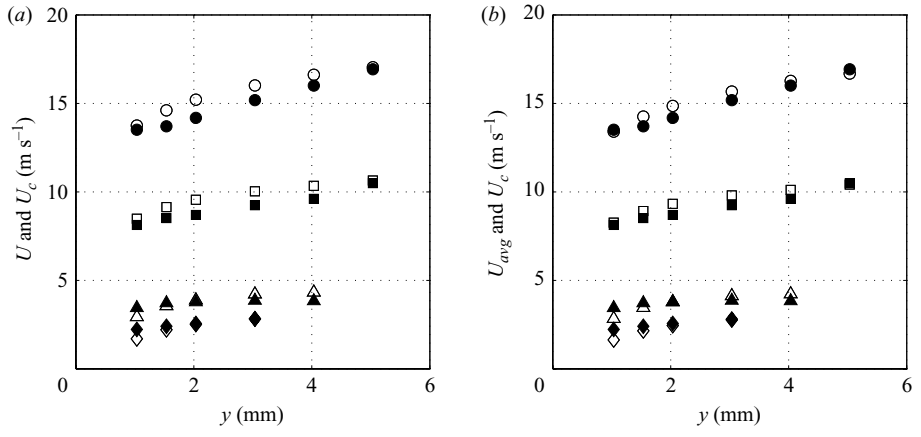

FIGURE 24. Comparison of the convection velocity $U_c(y)$ with (*a*) the local mean velocity $U(y)$ and (*b*) the average mean velocity $U_{avg}(y)$, for different pressure gradients: ○ and ●, PG1; □ and ■, PG3; △ and ▲, PG6; ◇ and ◆, PG8. The solid symbols indicate $U_c(y)$, and the hollow symbols indicate $U(y)$ or $U_{avg}(y)$.

seen that the variation of convection velocity with y is similar to that observed by Österlund (1999) in a ZPG flow. Further it may be observed that for all the pressure gradients, $U_c(y)$ is always of the order of 90 % of $U(y)$.

It was noted in the last paragraph of § 6 that the local mean velocity and hence the convection velocity are not strictly constant in the streamwise direction because of the presence of the streamwise pressure gradient. Thus we may interpret the measured convection velocity $U_c(y)$ to be the 'average' convection velocity, where the average is taken over the range of Δx values from which $U_c(y)$ is calculated. It therefore appears more appropriate to compare $U_c(y)$ with the *average* local mean velocity $U_{avg}(y)$ where the average is taken, say, over streamwise spatial separation $\Delta x_0 = 40$ mm between the SHW and HW probes. Figure 24(*b*) shows the comparison of $U_c(y)$ and $U_{avg}(y)$. It is clear from figure 24(*a*, *b*) that $U_c(y)$ indeed agrees more closely with $U_{avg}(y)$ than with $U(y)$, indicating that the spatial averaging is taking place.

We may now conclude that the experimentally determined local convection velocity $U_c(y)$ is not very different from the local mean velocity (of the order of 90 % of $U(y)$) at least over the range of wall-normal distance covered in this exercise. Since the structure under consideration is a large-scale structure, this finding is not inconsistent with those of Krogstad *et al.* (1998), Dennis & Nickels (2008) and Österlund (1999) even though the flow under investigation in those cases was a ZPG turbulent boundary layer flow. This justifies the use of local mean velocity as convection velocity in the present study while using Taylor's hypothesis and indicates that a typical structure in the present study gets convected downstream almost along with the mean flow.

8. Conclusions

In the current paper, various aspects of the large-scale structure in turbulent and reverse-transitional boundary layers subjected to streamwise FPGs have been investigated. The so-called sink flow configuration has been used to study these boundary layers, since this type of flow is in 'perfect equilibrium' in the sense of Townsend (1956, 1976) and Rotta (1962). The use of sink flow configuration allows systematic characterization of the large-scale structure with the strength of the FPG as a parameter where the characterization is not contaminated by the upstream history effects.

The large-scale structure is identified by cross-correlating the wall-shear stress fluctuation with the streamwise velocity fluctuation. The structure orientation is found to be linear over a large wall-normal extent typically extending from $y/\delta = 0.1$ to $y/\delta = 0.6$. Beyond $y/\delta = 0.6$, the correlation under consideration becomes very weak to allow any conclusive result. The average structure inclination angle α_{avg} is found to decrease systematically with increase in the streamwise FPG. This result is important and has implications towards modelling of the near-wall region. Further it is found that the structure gets elongated considerably as the FPG is increased, i.e. the streamwise spatial extent of the structure increases. Taken together, it is observed that the structure becomes flatter and longer with the increase in the FPG. Structural models are proposed for sink flow turbulent boundary layers in the form of either the shape of individual hairpin vortices or the possible structural self-organization. These models are then discussed in the light of the present experimental results. It is also shown that the process of relaminarization of a turbulent boundary layer by a strong FPG (the so-called soft relaminarization) may be better appreciated by appealing to these structural models.

The validity of Taylor's hypothesis for structure angle measurements in the present study has been established experimentally. This exercise is important because the flows under consideration are highly accelerated and are sometimes even reverse transitional. In most of the previous work on the validity of Taylor's hypothesis, at least for the measurements similar to the present work, emphasis has been on ZPG turbulent boundary layers. The present exercise is therefore crucial for accelerating flows. Possible reasons for the observed validity of Taylor's hypothesis have also been identified – specifically it is seen that the condition $\Delta x_p/L' \ll 1$ needs to be met for Taylor's hypothesis to be valid in pressure gradient flows, where $L' = U_\infty/(\mathrm{d}U_\infty/\mathrm{d}x)$ is the length scale which the streamwise pressure gradient introduces and Δx_p is the projection distance in Taylor's hypothesis (see figure 1*b*).

The investigation of structure convection velocity from space–time correlations has revealed that the convection velocity in the present work is fairly close to the local mean velocity of the flow (more than 90 %), which implies that the structure gets convected downstream almost along with the mean flow.

REFERENCES

Adrian, R. J., Meinhart, C. D. & Tomkins, C. D. 2000 Vortex organization in the outer region of the turbulent boundary layer. *J. Fluid Mech.* **422**, 1–54.

Blackwelder, R. F. & Kovasznay, L. S. G. 1972 Large-scale motion of a turbulent boundary layer during relaminarization. *J. Fluid Mech.* **53**, 61–83.

Bradshaw, P. & Wong, F. Y. F. 1972 The reattachment and relaxation of a turbulent shear layer. *J. Fluid Mech.* **52**, 113–135.

Brown, G. L. & Thomas, A. S. W. 1977 Large structure in a turbulent boundary layer. *Phys. Fluids* **20** (10), S243–S252.

Chauhan, K. A., Nagib, H. M. & Monkewitz, P. A. 2007 Evidence on non-universality of Kármán constant. In *Progress in Turbulence II: Proceedings of the iTi Conference in Turbulence 2005* (ed. M. Oberlack, G. Khujadze, S. Günther, T. Weller, M. Frewer, J. Peinke & S. Barth), Springer Proceedings in Physics, pp. 159–163. Springer.

Christensen, K. T. & Adrian, R. J. 2001 Statistical evidence of hairpin vortex packets in wall turbulence. *J. Fluid Mech.* **431**, 433–443.

Clauser, F. H. 1956 The turbulent boundary layer. *Adv. Appl. Mech.* **4**, 1–51.

Colella, K. J. & Keith, W. L. 2003 Measurements and scaling of wall shear stress fluctuations. *Exp. Fluids* **34**, 253–266.

Coles, D. E. 1956 The law of the wake in the turbulent boundary layer. *J. Fluid Mech.* **1**, 191–226.

Coles, D. E. 1957 Remarks on the equilibrium turbulent boundary layers. *J. Aerosp. Sci.* **24**, 495–506.

DeGraaff, D. B. & Eaton, J. K. 2000 Reynolds-number scaling of the flat-plate turbulent boundary layer. *J. Fluid Mech.* **422**, 319–346.

Dennis, D. J. C. & Nickels, T. B. 2008 On the limitations of Taylor's hypothesis in constructing long structures in a turbulent boundary layer. *J. Fluid Mech.* **614**, 197–206.

Dixit, S. A. & Ramesh, O. N. 2008 Pressure-gradient-dependent logarithmic laws in sink flow turbulent boundary layers. *J. Fluid Mech.* **615**, 445–475.

Ganapathisubramani, B., Hutchins, N., Hambleton, W. T., Longmire, E. K. & Marusic, I. 2005 Investigation of large-scale coherence in a turbulent boundary layer using two-point correlations. *J. Fluid Mech.* **524**, 57–80.

Ganapathisubramani, B., Longmire, E. K. & Marusic, I. 2003 Characteristics of vortex packets in turbulent boundary layers. *J. Fluid Mech.* **478**, 35–46.

Head, M. R. 1976 Eddy viscosity in turbulent boundary layers. *Aeronaut. Quart.* **27**, 270–276.

Head, M. R. & Bandyopadhyay, P. 1981 New aspects of turbulent boundary-layer structure. *J. Fluid Mech.* **107**, 297–338.

Hussain, A. K. M. F. 1983 Coherent structures – reality and myth. *Phys. Fluids* **26** (10), 2816–2850.

Hutchins, N., Nickels, T. B., Marusic, I. & Chong, M. S. 2009 Hot-wire spatial resolution issues in wall-bounded turbulence. *J. Fluid Mech.* **635**, 103–136.

Jones, M. B., Marusic, I. & Perry, A. E. 2001 Evolution and structure of sink-flow turbulent boundary layers. *J. Fluid Mech.* **428**, 1–27.

Krogstad, P. Å., Kaspersen, J. H. & Rimestad, S. 1998 Convection velocities in a turbulent boundary layer. *Phys. Fluids* **10** (4), 949–957.

Krogstad, P. Å. & Skåre, P. E. 1995 Influence of a strong adverse pressure gradient on the turbulent structure in a boundary layer. *Phys. Fluids* **7** (8), 2014–2024.

Le, H., Moin, P. & Kim, J. 1997 Direct numerical simulation of turbulent flow over a backward-facing step. *J. Fluid Mech.* **330**, 349–374.

Lee, J. H. & Sung, S. J. 2009 Structures in turbulent boundary layers subjected to adverse pressure gradients. *J. Fluid Mech.* **639**, 101–131.

Ligrani, P. M. & Bradshaw, P. 1987 Spatial resolution and measurement of turbulence in the viscous sublayer using subminiature hot-wire probes. *Exp. Fluids* **5**, 401–417.

Marusic, I. 2001 On the role of large-scale structures in wall turbulence. *Phys. Fluids* **13** (3), 735–743.

Marusic, I. & Heuer, W. D. C. 2007 Reynolds number invariance of the structure inclination angle in wall turbulence. *Phys. Rev. Lett.* **99** (114504), 1–4.

Marusic, I., Kunkel, G. J. & Porté-Agel, F. 2001 Experimental study of wall boundary conditions for large-eddy simulation. *J. Fluid Mech.* **446**, 309–320.

Narasimha, R. 1983 Relaminarization – magnetohydrodynamic and otherwise. *Progr. Astronaut. Aeronaut.* **84**, 30–52.

Narasimha, R. & Sreenivasan, K. R. 1973 Relaminarization in highly accelerated turbulent boundary layers. *J. Fluid Mech.* **61**, 417–447.

Narasimha, R. & Sreenivasan, K. R. 1979 Relaminarization of fluid flows. *Adv. Appl. Mech.* **19**, 221–309.

Nickels, T. B. 2004 Inner scaling for wall-bounded flows subject to large pressure gradients. *J. Fluid Mech.* **521**, 217–239.

Österlund, J. M. 1999 Experimental studies of zero pressure-gradient turbulent boundary layer flow. PhD thesis, Department of Mechanics, Royal Institute of Technology (KTH), Stockholm.

Perry, A. E. & Chong, M. S. 1982 On the mechanism of wall turbulence. *J. Fluid Mech.* **119**, 173–217.

Perry, A. E., Henbest, S. & Chong, M. S. 1986 A theoretical and experimental study of wall turbulence. *J. Fluid Mech.* **165**, 163–199.

Perry, A. E., Marusic, I. & Jones, M. B. 2002 On the streamwise evolution of turbulent boundary layers in arbitrary pressure gradients. *J. Fluid Mech.* **461**, 61–91.

Perry, A. E., Marusic, I. & Li, J. D. 1994 Wall turbulence closure based on classical similarity laws and the attached eddy hypothesis. *Phys. Fluids* **6**, 1024–1035.

Piomelli, U., Ferziger, J., Moin, P. & Kim, J. 1989 New approximate boundary conditions for large eddy simulations of wall-bounded flows. *Phys. Fluids* **A1** (6), 1061–1068.

Robinson, S. K. 1991 Coherent motions in the turbulent boundary layer. *Annu. Rev. Fluid Mech.* **23**, 601–639.

Rotta, J. C. 1962 Turbulent boundary layers in incompressible flow. *Progr. Aeronaut. Sci.* **2**, 1–220.

Saddoughi, S. G. & Veeravalli, S. V. 1994 Local isotropy in turbulent boundary layers at high Reynolds number. *J. Fluid Mech.* **268**, 333–372.

Schlichting, H. & Gersten, K. 2000 *Boundary-Layer Theory*, 8th edn. Springer.

Spalart, P. R. & Leonard, A. 1987 Direct numerical simulation of equilibrium turbulent boundary layers. In *Turbulent Shear Flows 5* (ed. F. Durst, B. E. Launder, J. L. Lumley, F. W. Schmidt & J. H. Whitelaw), pp. 234–252. Springer.

Sreenivasan, K. R. 1981 Relaminarizing flows (data evaluation). In *The 1980-81 AFOSR-HTTM Stanford Conference on Complex Turbulent Flows: A Comparison of Computation and Experiment* (ed. B. J. Cantwell, S. J. Kline & G. M. Lilley), vol. II, pp. 567–581. Stanford University Press.

Sreenivasan, K. R. 1982 Laminarescent, relaminarizing and retransitional flows. *Acta Mech.* **44**, 1–48.

Taylor, G. I. 1938 The spectrum of turbulence. *Proc. R. Soc.* A **164**, 476–490.

Tennekes, H. & Lumley, J. L. 1972 *A First Course in Turbulence*. MIT Press.

Townsend, A. A. 1956 *The Structure of Turbulent Shear Flow*, 1st edn. Cambridge University Press.

Townsend, A. A. 1976 *The Structure of Turbulent Shear flow*, 2nd edn. Cambridge University Press.

Uddin, A. K. M., Perry, A. E. & Marusic, I. 1997 On the validity of Taylor's hypothesis in wall turbulence. *J. Mech. Engng Res. Dev.* **19–20**, 57–66.

Wark, C. E. & Nagib, H. M. 1991 Experimental investigation of coherent structures in turbulent boundary layers. *J. Fluid Mech.* **230**, 183–208.

Wu, X. & Moin, P. 2009 Direct numerical simulation of turbulence in a nominally zero-pressure-gradient flat-plate boundary layer. *J. Fluid Mech.* **630**, 5–41.